Phenomena on Bipolar Junction Transistors in Space

In-Situ Data to Further Humankind's Quest for Expansion

by

Adalin Benedetto

A Thesis Presented in Partial Fulfillment
of the Requirements for the Degree
Master of Science

Approved January 2023 by the
Graduate Supervisory Committee:

Hugh Barnaby, Chair
Stephen Goodnick
Ivan Sanchez Esqueda

ARIZONA STATE UNIVERSITY

May 2023

ABSTRACT

Linear bipolar circuits, designed with bipolar junction transistors (BJTs), are particularly vulnerable to the effects of space radiation. These circuits, which are usually commercial off-the-shelf (COTS) components, typically exhibit Enhanced Low Dose Rate Sensitivity (ELDRS), which is characterized by the enhancement of degradation when parts are exposed to radiation at low dose rates as compared to high dose rates. This phenomenon poses significant problems for the qualification of bipolar parts for use in low dose rate environments, such as most Earth orbits. ELDRS in BJTs has been well-documented in ground-based experiments; however, the effects of low dose rate irradiation on bipolar transistors manufactured in an integrated linear process had never been characterized in space - until the ELDRS experiment was launched in June 2019. The ELDRS instrument measures changes in the active collector and base currents in 24 lateral PNP (LPNP) BJTs on eight packaged die (three BJTs per die). Sixteen of the 24 BJTs are gated, while eight are standard, un-gated LPNPs. Device Under Test (DUT) and measurement variables include oxide thickness, passivation layer, packaging conditions, and gate voltage. This thesis reports the results obtained after more than 20 months of space flight in a highly elliptical Earth orbit. These results demonstrate that this category of bipolar devices is susceptible to low dose rate exposures and therefore exhibits the ELDRS effect in an actual space environment. This thesis also assess the impact of packaging variables on radiation response and examines one of the major causes behind radiation degradation, interface traps. An understanding of radiation effects in real space environments is critical for future missions that use these low-cost COTS bipolar technologies, making these results highly relevant for the satellite community.

TABLE OF CONTENTS

Page

LIST OF TABLES....................iii

LIST OF FIGURES....................iv

CHAPTER

1 INTRODUCTION....................1

2 SPACE ENVIRONMENT, IONIZING RADIATION, AND EFFECTS ON SEMICONDUCTOR DEVICES....................6

a. The Tempestuous Space Environment....................6

b. Ionizing Radiation....................12

c. Bipolar Junction Transistors....................16

3 EXPERIMENTAL DETAILS....................21

a. Background....................21

b. Data Collection and Analysis Process....................31

4 EXPERIMENTAL RESULTS....................37

a. ELDRS Results....................37

b. Package and Test Condition Variables....................41

c. SRV and NIT Extraction....................50

d. Linear Regression Analysis....................56

5 CONCLUSION....................60

REFERENCES....................62

LIST OF TABLES

Table Page

1. Device Configurations....23

2. Variables Associated With Experimental Parameters 41

3. Dose And Corresponding srv Values 51

LIST OF FIGURES

Figure Page

1. Example LEO Orbital Inclination, 3D And Grid Representations..............................8

2. Earth's Magnetic Dipole Field And Magnetic Vs. Geographic Pole Offset.................9

3. Dose (rad) Vs. Spacecraft Shielding Thickness (mm) For An Example LEO Orbit..12

4. Flux ($cm^{-2} \cdot s^{-1} \cdot MeV^{-1}$) Vs. Energy (MeV) For LEO Orbit 13

5. ELDRS Lot Acceptance Flow Chart...15

6. PNP-Type BJT Schematic Representation And Circuit Diagram Symbol...............16

7. ELDRS Instrument, Front And Back PCB...21

8. GLPNP Layout..22

9. DUT Chip Pad Allocations/IC Pinout...23

10. PCB Operation For DUT Measurement...24

11. ELDRS Flight Board Block Diagram..25

12. VA2/VRAMP Schematic..26

13. I-V Converter Schematic..27

14. ELDRS Test Output, Voltage (V) Vs. Time (s)..29

15. Accumulated Average Ionizing Dose (krad) Vs. Date Over The Duration Of The Experiment...30

16. Data Analysis GUI Output...31

17. Temperature (K) Vs. Date For The Duration Of The Experiment...........................33

18. GLPNP Thick Oxide Simulation Structure...34

Figure Page

19. Relative Damage Vs. Dose Rate (rad(Si)/s)....................37

20. ΔI_B (nA) Vs. Total Dose (krad(Si)) For The Duration Of The Experiment....................39

21. Thick Oxide, Modified P-Glass Vs. Unmodified P-Glass, 0V And -12V....................44

22. Sic Modified Package, Thick Oxide Vs. Thin Oxide, 0V And -12V....................45

23. P-Glass Modified Package, Thick Oxide Vs. Thin Oxide, 0V And -12V....................46

24. Thick Oxide, P-Glass Modified Vs. Sic Modified, 0V And -12V....................47

25. Simulated I_B Vs. V_{EB} For T=300 K....................50

26. N_{IT} (cm^{-2}) Vs. Dose (krad)....................52

27. NPN Metal-Oxide Connection....................53

28. Thin Oxide At V_G = 0 V And -12 V....................54

29. Thick Oxide At V_G = 0 V And -12 V....................54

30. Log(I_B) (nA) Vs. V_{EB} (V), GLPNP, Pre- And Post-Irradiation....................57

31. Log(I_B) (nA) Vs. V_{EB} (V), GLPNP, Post-Irradiation....................58

CHAPTER 1

INTRODUCTION

Spacecraft have a difficult task: to survive in an environment hostile to delicate electronic parts while reliably fulfilling their purpose of sending data back to Earth so that humankind can continue their millennia-long quest to expand beyond known limits. Many spacecraft electronics rely on linear bipolar circuits, made with common bipolar parts. Linear bipolar parts, often transistors fabricated in a linear bipolar process such as operational amplifiers, voltage regulators, and comparators, are designed with bipolar junction transistors (BJTs). This is especially true of analog instruments used in spacecraft electronics, where the long flight heritage, continued effectiveness, and the ubiquity of linear bipolar technologies play a major role in part selection. Unfortunately, BJTs are particularly vulnerable to the harmful effects of high ionizing-radiation environments such as those in electron- and proton- rich, low dose rate Earth orbits [1, 2, 3, 4] where most spacecraft are intended to fly. These parts are susceptible to degradation due to total ionizing dose (TID) radiation as well as enhanced low dose rate sensitivity (ELDRS), which can cause serious degradation or failure, or at best simply shorten the lifetime of active semiconductor components [5], limiting mission lifetimes.

While many effects in transistors can be mitigated with a well-designed circuit, total-dose failure mechanisms can still have deliterious effects [6]. Radiation-hardened parts, specifically designed to be more resistant to radiation-induced degradation, are available; but can be prohibitively expensive, have long lead times, and are often out of stock due to supply chain or production complications. For this reason, commercial-off-the-shelf

(COTS) parts are most often used in spacecraft designs, despite being highly susceptible to damage from ionizing radiation.

The primary characteristic of TID-induced degradation in BJTs is an increase in base current (IB), attributed to the buildup of defects at or near the oxide interface with underlying silicon. As semiconductor devices are processed with very deliberate amounts of defects in the materials for ideal operation, introducing unwanted defects can cause malfunction or total failure of the parts and circuits.

Degradation due solely to radiation can be difficult to determine with space data since degradation is closely linked to both radiation dose and temperature. In space environments, extreme temperature fluctuations are expected. Temperature will also change IB, which makes it difficult to determine whether the changes in base current are due to temperature or radiation. The temperature fluctuations necessitate a BJT model to separate the temperature from the radiation effects. Chapter 2 provides a description of the space environment as well as the effects of ionizing radiation on semiconductor devices, specifically bipolar junction transistors. In Chapter 3, the response of BJTs to ionizing radiation is detailed using the data gathered from space and a model created to separate thermal from radiative effects.

Ground-based testing has successfully produced the ELDRS response in bipolar junction transistors. However, ground-based dose rate testing and qualification is particularly difficult due to the long test times resulting from the very low dose rate necessary. For example, a qualification experiment that could take three minutes using a standard high dose rate (HDR) radiation source ((MIL-STD-883 TM1019 Condition A 50-300 rad/s) may take more than four months to perform in a low dose rate (LDR) source (10 mrad/s).

Additionally, parts in flight have been shown to degrade more quickly due to the added effects of proton damage, the complex variations in environment including unpredictable space weather events, and very high energy particles that complicate characterization of spacecraft shielding, all of which cannot easily be replicated in ground-based tests [5]. To further complicate environment characterization and part qualification, hardly any data has been gathered on the exact composition of the environment far from Earth, where future missions to Mars are (optimistically) anticipated as soon as 2037 [7].

Space environments are composed of a complex cocktail of particles including electrons and protons of varying energies. Damage to parts and circuits in space is caused by exposure to this harsh radiation environment as well as extreme, wildly fluctuating temperatures. The space environment, particularly in popular spacecraft orbits, has been characterized using previous mission data to create models that estimate the dose a mission will receive. Qualification of parts involves predicting the dose and particles that the mission will encounter, generally using environment models, then using available previous testing data or performing new qualifying tests to determine whether the parts will be able to survive, and accounting for the unquantified higher doses in real environments with large design margins.

Although test and design margins have been shown to bound ELDRS response in BJTs for ground-based testing, further characterization of both the space environment and ELDRS mechanism in BJTs will be important for future missions, as longer missions to explore Mars and beyond are nearing. The analysis in this thesis of data gathered from the BJTs in space will facilitate a more in-depth understanding of the way that radiation can affect materials and fabrication processes for improved part qualification in the future via

development and improvement of models designed to simulate radiation degradation in transistors.

Data from actual space missions is sparse. Space data is historically difficult to collect, largely due to program costs. The Microelectronics and Photonic Testbed (MPTB), launched in 1997, demonstrated ELDRS in linear bipolar circuits in flight [8, 9]. This only previous in-flight ELDRS experiment demonstrated increased parametric degradation in linear bipolar parts and mostly validated the efficacy of test methods on these circuit types. The MPTB is considered to be an unqualified success due to its unprecedented demonstration of ELDRS in an actual space environment, validating that current ELDRS qualification techniques adequately bound the response of specific linear bipolar circuits and its enabling of analysis of the impact of space-based protons and other high energy particles on the performance of linear bipolar parts.

NASA's Living With a Star Space Environment Testbed experiment furthers this accomplishment by acquiring data for individual COTS BJT devices that are fundamental elements of linear bipolar parts, which have comparable ground-based data. In addition to furthering test validity and impacting future screening/processing effectiveness, these space data has given insight into the physical mechanisms of degradation. The devices under test (DUTs) were designed with variations in the packaging which have been compared to give insight into which conditions affect the radiation response. Additionally, among the most destructive of defects, interface traps (NIT), have been studied, which increase surface recombination and lead to a precipitous rise in base current (IB) [6, 10, 11], and are discussed in chapter 4. A measured change in IB can provide insight to the buildup of these traps via extraction of a BJT's surface recombination velocity (srv), which

can then be plugged into an analytical model to obtain a quantitative simulation of the NIT buildup [11]. More information from space data about how these traps are generated and under what conditions will lead to improved models for simulating the TID response of BJTs, allowing for more targeted testing and less testing overall, improving mission estimates and reducing costs both from testing and by being able to continue using COTS parts.

Direct measurements in space of the effects of LDR irradiation on individual bipolar transistors manufactured on an integrated linear process had never been performed until the ELDRS experiment on the NASA Living With a Star (LWS) Space Environment Testbed (SET), launched June 2019 from the Kennedy Space Center on a SPACEX Falcon Heavy. Space data is crucial to better understanding the intricate space environment, the physics of degradation in parts, and the effectiveness of ground-based testing for predicting the degradation of parts in space. Analysis of these data has given insight into how differences in packaging and materials can affect the post-irradiation base current response and also supports the validation of existing models for ELDRS and proton effects in bipolar components, enhances understanding of the correlation of space radiation effects and ground test data, enables validation or improvement of test procedures for ground-based hardness assurance testing, and ultimately takes steps toward the development of radiation hardening methodologies that mitigate the damaging effects of solar and trapped protons in earth-orbiting and space exploration systems.

CHAPTER 2

SPACE ENVIRONMENT, IONIZING RADIATION, AND EFFECTS ON SEMICONDUCTOR DEVICES

a. The Tempestuous Space Environment

The space environment is highly complex. Fully characterizing mission environments and accurately predicting acquired radiation dose are practically impossible, as the exact environment depends on the amount of each particle type present, as well as its energy and direction, random events such as magnetic storms or solar flares or coronal mass ejections (CMEs), spacecraft and packaging shielding, and natural variations in the cosmic background and galactic cosmic rays (GCRs) [8]. Due to the impossibility in accounting for all these factors, estimating the acquired dose for each mission is usually performed using empirical models of space radiation flux, discussed further in this section, which are often created from data previously gathered using dosimeters. Accurate estimate of mission lifetime dose is important for calculating the survivability of the mission, selecting parts appropriately, calculating necessary shielding, and other mitigation techniques.

Charged particles, which are omnipresent in space, are a threat to electronics both via total ionizing dose (TID), the total dose accumulated over the lifetime of the mission; displacement damage (DD), damage caused in the structure by large particles; and single event effects (SEEs), failure or interruption due to a single charged particle strike . The technique for measuring SEEs (involving examining the voltage and current outputs over the entire exposure period) has not been enabled in this experiment, and discussion herein focuses only on cumulative radiation damage, which includes TID- and DD-induced

degradation . Although some research has been conducted as to whether degradation is correlated with TID and SEE, the failure mechanisms do not tend to overlap. As such, confusing SEE failures for TID degradation was not a concern in this experiment.

The environments where Earth missions are flown are identified by the orbit, which is defined by height above the Earth and path followed around it. Each orbit has its own composition of particles. Very close to the Earth, such as the low-Earth orbit (LEO) where the International Space Station (ISS) resides, Earth's atmosphere protects spacecraft from some percentage of particles, making it the least harsh environment in which to fly. LEO reaches an altitude of about 2000 km and is nearly circular [12]. Many missions are also flown in medium Earth orbit (MEO) and high Earth orbit/highly elliptical orbit (HEO), also known as geostationary Earth orbit (GEO), which are much more hostile to electronic devices. Satellites in HEO/GEO fly at the same speed as the Earth, making it a geostationary orbit. GEO is about 22,200 km above the Earth and is the orbit used by the global positioning system (GPS) satellites due to providing a constant view of the Earth and following a consistent and highly predictable path [12]. Shown in Fig. is a typical LEO orbit, generated using OMERE v.5.6.1.

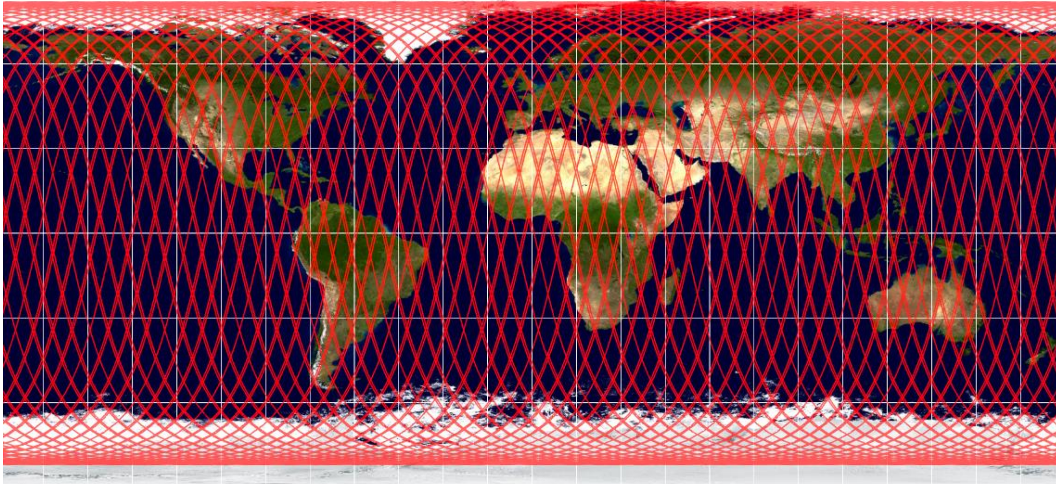

Figure 1. Example LEO orbital inclination, 3D and grid representations

The magnetic field around the Earth, called the geomagnetic field or magnetosphere traps charged particles that enter it from solar winds or GCRs. Earth has two primary zones of charged particles: the outer radiation belt and the inner radiation belt, called the Van Allen Belts. The Van Allen belts are primarily composed of protons between 100 keV and several hundred MeV and electrons with energies between ~10 keV and 10 MeV [[13]], both with plenty of energy to disturb electronic devices. Due to their differing mass, electrons tend to collect in the inner shell, and protons in the outer shell. Protons can be emitted from solar flares or cosmic rays. Both the proton and electron concentrations in the belts can vary wildly, with even a third belt appearing and disappearing in 2013 [14]. The energy of particles in the belts can also vary with random space events such as solar storms. The Van Allen Belts are arranged according to the dipole magnetic field surrounding the Earth, shown in Figure 2 [12]. The Earth's magnetic north pole and geographic north pole are slightly offset, also shown in Figure 2.

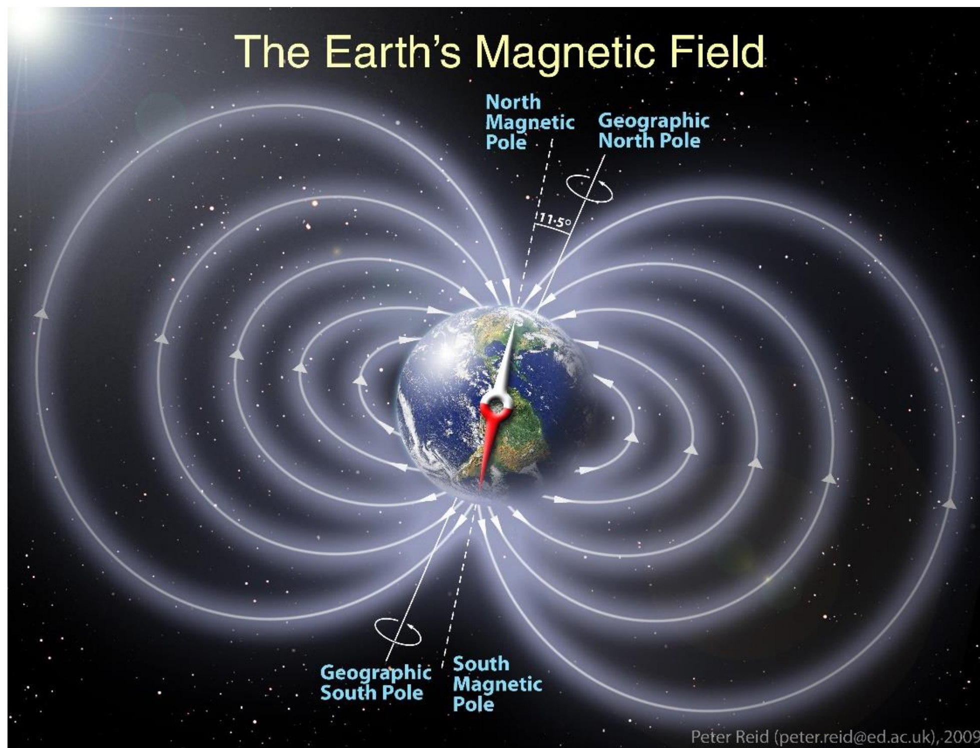

Figure 2. Earth's magnetic dipole field and magnetic vs. geographic pole offset

The asymmetry of the belts can also create unpredictability that poses threats to spacecraft. The South Atlantic Anomaly (SAA), located over the south Atlantic, is a variation in the Van Allen belts due to the offset between magnetic and geographic north (as seen in Figure 2). The SAA is a region where the Van Allen radiation belts dip close to the Earth, causing an increase in flux and exposing satellites in LEO to a higher level of ionizing radiation. The Van Allen Belts also dip close to the Earth at the poles, which causes the aurora borealis, a beautifully eerie display of visible light caused by photons emitted from ions entering Earth's atmosphere.

Radiation environment variability can be caused by unpredictable events including: solar flares; storms, and wind; coronal mass ejections (CMEs), a localized magnetic explosion above the surface of the sun; distant neutron star explosions; and varying galactic cosmic ray (GCR) background radiation [15]. The environment is also variable due to the 11-year solar cycle, which involves 7 years of high activity levels, referred to as solar maximum, and 4 years of lower activity, called solar minimum [15].

The extreme temperature conditions in space are also unfriendly to electronics. The temperature fluctuates wildly in orbit, largely due to the geographic inevitability of crossing the sun's path. Temperature significantly affects the base current response in BJTs, which poses difficulty not only for mission qualification but also for analysis of space data, necessitating the separation of temperature and radiation effects. Additionally, many COTS parts are not qualified for usage in extreme temperatures.

Relatively accurate models have been developed to predict the dose a spacecraft will receive for specific parameters, using data gathered from experiments flown with dosimeters that record dose. It has been shown that p-channel metal-oxide semiconductor field effect transistors (MOSFETs) can be used as accurate radiation dosimeters, and have since been commonly used to measure accumulated dose in varying orbits [16]. Data on shielding in space has also been collected. A space mission called the Trapped Ions in Space (TRIS) experiment, flown in 1984, helped define the LET spectrum at different thicknesses of shielding using a stack of plastic track detectors [17]. TRIS reaffirmed that the measured LET flux tends to exceed predictions [17].

The standard proton and electron population models are NASA's AP-8 and AE-8, respectively. They are based on data gathered in the 1960's-70's and have been the standards for many years. These models include solar maximum/minimum flux as well as other options that can be selected to create the most accurate prediction of accumulated dose for the specified mission [18]. The European Space Agency (ESA)'s Space Environment Information System (SPENVIS) and NASA/Vanderbilt's Cosmic Ray Effects on Micro-Electronics (CREME96), and TRAD's OMERE are common programs that use the standard charged particle models for modeling the ionizing radiation environment and its predicted effects on a given mission. The calculation considers the lifetime of the mission, orbital trajectory or path above the earth (inclination), orbital altitude (apogee and perigee), and launch date. Many space programs use a compilation of these tools and others to obtain the most accurate depiction possible.

Shown in Figure 3 is a graph of received dose vs. spacecraft shielding thickness, created using OMERE, for a circular LEO orbit with an apogee (maximum distance from Earth) of 800 km, perigee (minimum distance from Earth) of 800 km, inclination of 98°, and 10 year mission duration. This graph shows how electrons (purple line) are more easily stopped with shielding, whereas solar protons (orange line) and secondary photons (green line) are not. The blue line at the very top represents total accumulated dose. It rises only slightly above the solar proton curve, demonstrating how solar protons are a particular threat to spacecraft due to their large mass and higher energy, meaning they are not easily blocked by shielding. Protons are also responsible for both ionization and displacement effects in many bipolar parts and circuits, making them a notable concern

.

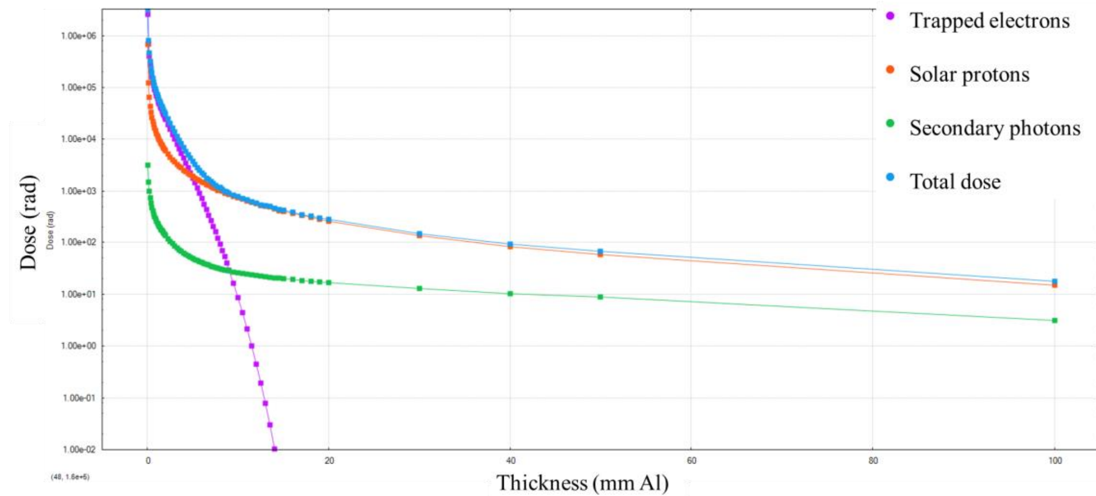

Figure 3. Dose (rad) vs. spacecraft shielding thickness (mm) for an example LEO orbit

Updated electron and proton population models AE-9 and AP-9 have been released more recently, which extend spatial resolution as well as better uncertainty quantification and confidence levels [18]. However, even the best models are not able to fully account for spatial and temporal variations; additionally, these highly complex calculations can take considerable computing power. For these reasons space-based qualification is preferred to ground-based when possible, and gathering as much space data as possible is critical for developing and improving models [[13]].

b. Ionizing Radiation

Radiation is composed of subatomic particles and electromagnetic waves. Much radiation is non-harmful to either humans or electronics, as it lacks enough energy to interact on the atomic level. Ionizing radiation is a particular type of radiation that possesses sufficient

energy to produce electron-hole pairs (ehp), called ionization. A charged particle leaves a charged path through the material as a result of the energy released when a highly energetic carrier collides with the crystal lattice in semiconducting materials. The amount of energy that an ionizing particle transfers to the material along its path is referred to as linear energy transfer (LET) and is measured in energy deposited per unit length (common units for radiation testing are MeV/cm). LET spectra for the same LEO orbit as described above are shown in Figure 4. This graph displays AP8/AE8 solar maximum conditions.

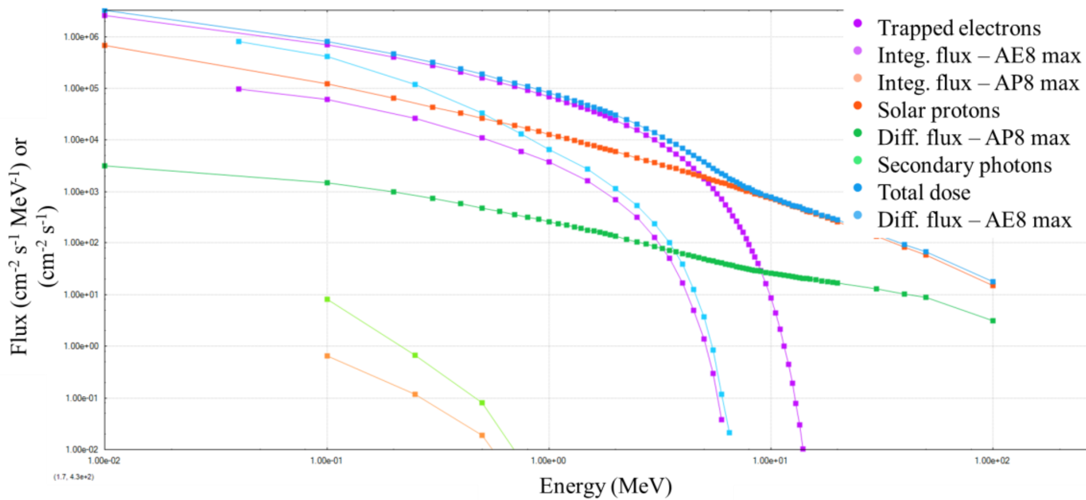

Figure 4. Flux (cm-2·s-1·MeV-1) vs. energy (MeV) for LEO orbit

Incident radiation can be made up of common ionizing particles that include: alpha and beta particles of varying energies; neutrons, with a wide range of energies and a large mass; and secondary photons, commonly ejected from Bremsstrahlung radiation, i.e. charged particles hitting each other and releasing photons. Incident radiation in the space environment can also include ionized elements that naturally occur in space, such as Ar, Ne, and Xe; and high energy electromagnetic waves, e.g. photons and gamma rays. As

discussed in the space environment section, these particles can originate from solar winds and storms, background radiation, GCRs, or distantly exploding neutron stars; and speed through space or become trapped in a planet's magnetosphere. The total amount of ionizing radiation accumulated over a certain duration is referred to as total ionizing dose (TID). TID-induced damage can be permanent but is generally known to anneal. However, annealing can take a long time and is usually most effective at elevated temperatures, not available in space which tends to be extremely cold [19]. Annealing cannot be relied on for part recovery post-irradiation in a space environment.

The prohibitive expense in terms of cost and time of LDR, high energy, and radiation test sources necessitates test methods that do not rely solely on LDR testing for every mission. To compensate for this difficulty and help ensure mission survivability, a test method was developed using either of two accelerated tests: 10 mrad/s at room temperature with a design margin of two (i.e., the result at a given dose must be multiplied by two in order to bound the predicted response) or 10 rad/s at 100 °C with a design margin of three.

The widely adopted qualification process flow chart is shown in Figure 5 [20], involving a common test method, MIL-STD-883 TM-1019, and radiation lot acceptance (RLAT), also helping to account for variability in manufacturing processes. These common test margins, as well as large design margins, have been shown to be effective at bounding the low dose rate response of radiation damage. However, parts in flight tend to degrade more quickly due to the added effects of proton damage, ultra-high-energy ions, unaccounted-for flux from spatial variations; and LDR irradiation causes particular problems for bipolar devices, as discussed in the next section.

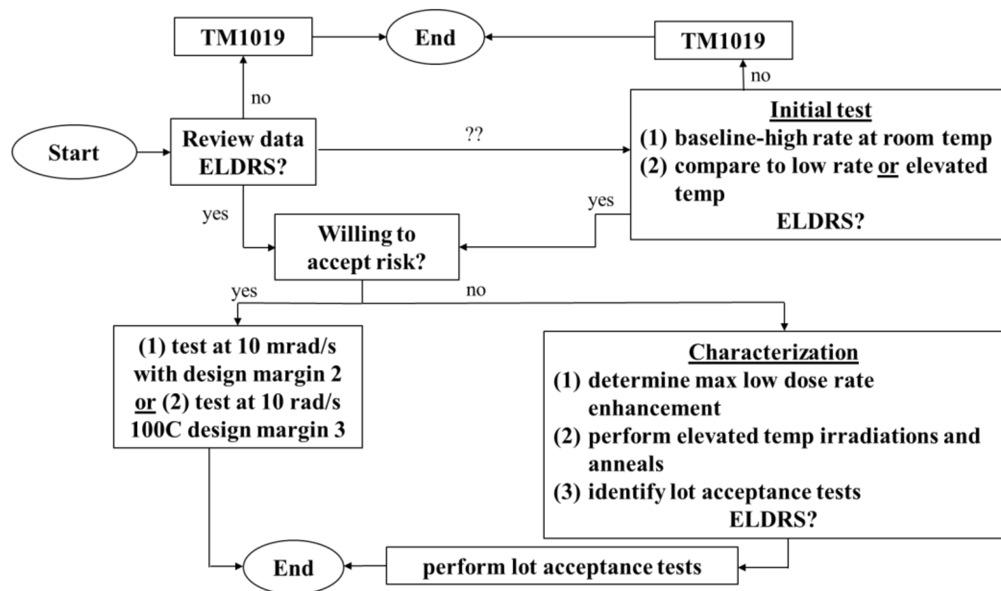

Figure 5. ELDRS lot acceptance flow chart

Technology computer assisted design (TCAD) models are also used to simulate ionizing radiation effects in BJTs. Computer models can be successfully used for preliminary screening but are not reliable enough yet for full qualification due to their own set of complications. First, bipolar devices have a non-uniform electric field at the oxide interface [21]. Additionally, the interface traps (NIT) that build up under ionizing radiation are also non-uniform [22]. Furthermore, manufacturing differences, even as seemingly inconsequential as slight variations in a single lot manufactured on the same wafer and process, can have significant consequences for the radiation response. More usefully, computer simulations can be run to support analysis of a transistor's radiation response characteristics, allowing srv and NIT to be calculated directly [22]. With more space data, computer models can be empirically improved to further support analysis of radiation response characteristics in semiconductors, particularly BJTs and LDR response.

c. Bipolar Junction Transistors

i. Background

Bipolar junction transistors are a type of semiconductor commonly used in both Earth-bound purposes and spacecraft, formed with two-junction/three-terminal transistor containing three adjoining, alternately doped regions [23]. A simplified diagram of the structure of a typical PNP BJT and circuit diagram symbol are shown in Figure 6 [23].

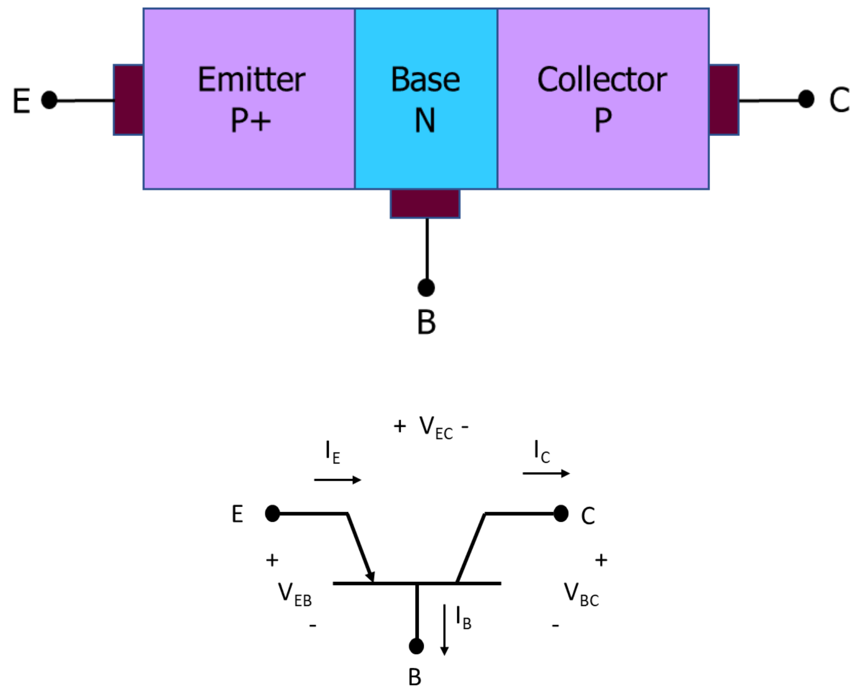

Figure 6. PNP-type BJT schematic representation and circuit diagram symbol

The width of the regions is carefully specified, with the base region designed to be much narrower than the diffusion length of minority carriers so that the carriers do not recombine before they can diffuse to the depletion layer of the other side of the junction, and with one side doped more heavily than the other to facilitate injection of holes [24]. Typical use involves the emitter junction being forward-biased, and injecting holes into the center base n-type region. The collector junction, so-called because it collects the injected holes from the emitter [24], is reversed-biased.

The structural characteristics of the transistor, particularly the doping levels and width of the base, can be manipulated to operate for different voltage conditions depending on the desired application, often conveniently used as amplifiers and switches of varying sizes and voltage requirements. Understanding the geometry of the BJT is paramount for understanding what is happening in the device when it is irradiated and why the degradation is caused. Bipolar junction transistors are a type of semiconductor commonly used in both Earth-bound purposes and spacecraft, formed with two-junction/three-terminal transistor containing three adjoining, alternately doped regions [23]. A simplified diagram of the structure of a typical PNP BJT and circuit diagram symbol are shown in Figure 6 [23].

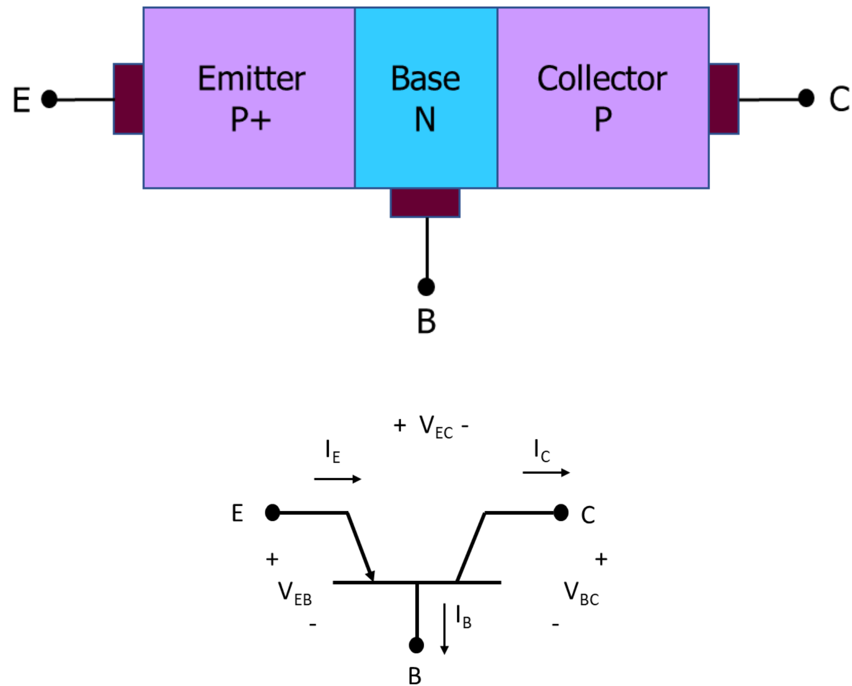

Figure 1. PNP-type BJT schematic representation and circuit diagram symbol

The width of the regions is carefully specified, with the base region designed to be much narrower than the diffusion length of minority carriers so that the carriers do not recombine before they can diffuse to the depletion layer of the other side of the junction, and with one side doped more heavily than the other to facilitate injection of holes [24]. Typical use involves the emitter junction being forward-biased, and injecting holes into the center base n-type region. The collector junction, so-called because it collects the injected holes from the emitter [24], is reversed-biased.

The structural characteristics of the transistor, particularly the doping levels and width of the base, can be manipulated to operate for different voltage conditions depending on the desired application, often conveniently used as amplifiers and switches of varying sizes and voltage requirements. Understanding the geometry of the BJT is paramount for

understanding what is happening in the device when it is irradiated and why the degradation is caused.

ii. Ionizing Radiation Response in BJTs

Damage from ionizing radiation, characterized by the increase in base current (I_B), is caused by a buildup of defects in the oxide and passivation layers above the bipolar base region [25, 6, 10, 21]. The “sensitive region” is near the oxide-silicon interface, where there is a high probability of surface carrier recombination via interface trap defects [25]. This increase in recombination with the interface traps causes a rise in base current. In forward bias in an ideal diode, collector current and base current are a function of Boltzmann’s factor $\frac{V_{EB}}{\phi_T}$ [25]:

$$I_C, I_B(ideal) \propto \exp\left(\frac{V_{EB}}{\phi_T}\right) \quad (1)$$

where $\phi_T = kT/q$ is the thermal voltage, comprised of Boltzmann’s constant (k), junction temperature (T), and electron charge (q). This equation shows the exponential dependence of I_B on both emitter-base bias and temperature, both significant variables in this experiment.

Oxide defects primarily interact with surface carrier concentrations within the base region, at the silicon-oxide interface of the emitter-base junction [22, 6]. Recombination centers at this location are related to the density of interface traps, which and are proportional to surface recombination velocity (s*rv*) [6]. Although NPN transistors tend

to be more sensitive to ionizing dose than PNP devices due to inversion in the p-doped base region [26], PNP transistors are typically more affected by LDR effects than NPN [5].

Gated diodes can be used to extract densities of radiation-induced oxide defects in BJTs directly by measuring surface recombination [6]. A gate on a lateral PNP (LPNP) can also be used to minimize degradation, i.e. base current increase, by varying the applied voltage V_G to either deplete the base, establishing an electric field that suppresses the generation of the oxide defects that increase recombination and in turn base current, or to put the device in accumulation mode, which decreases carrier recombination [11, 2000]. Gated diodes are also ideal for independently measuring the buildup of all of the defects associated with protons, thereby enabling the separation of displacement and ionization effects.

CHAPTER 3

EXPERIMENTAL DETAILS

a. Background

The "ELDRS" testbed experiment is of the four payloads on the Space Environment Testbeds (SET) mission developed through the NASA Living With a Star (LWS) program. The LWS program was designed to characterize the space environment to better understand its impact on the performance of electronics in space, validate the efficacy of the test method MIL-STD-883 TM 1019 testing recommendations, and reduce design margins. The main objective of the ELDRS testbed was to gather data on the effects of LDR space irradiation on individual linear BJTs, demonstrate the ELDRS effect on BJTs with LDR space irradiation, and assess the impact of experimental packaging parameters on radiation response. The testbed continuously measures radiation response of COTS bipolar device test structures by performing periodic measurements of base current (I_B) and collector current (I_C) as a function of emitter-base voltage (V_{EB}) and gate voltage (V_G) while recording several other related variables such as dose and temperature. These extracted current-voltage (I-V) characteristics enable the LDR effects on BJTs to be obtained in orbit. The test board measures the variables and current responses several times a month and records the data for download.

The testbed performs these measurements by inputting the exponentially changing currents through a logarithmic amplifier in response to the linear emitter voltage ramp (VRAMP) and converting them to be read out as linearly changing analog voltages. The data on both emitter voltage and base/collector current are retrieved from the analog output and stored for download in the testbed's main storage. The ELDRS instrument, shown in Figure 7, is

a 4”x6” double-sided printed circuit board (PCB) consisting of radiation tolerant measurement circuitry and 24 lateral PNP (LPNP) BJT devices under test (DUTs) that are integrated onto eight test chips (die), three BJTs per die, and packaged in hermetically sealed 14-pin dual inline packages (DIPs).

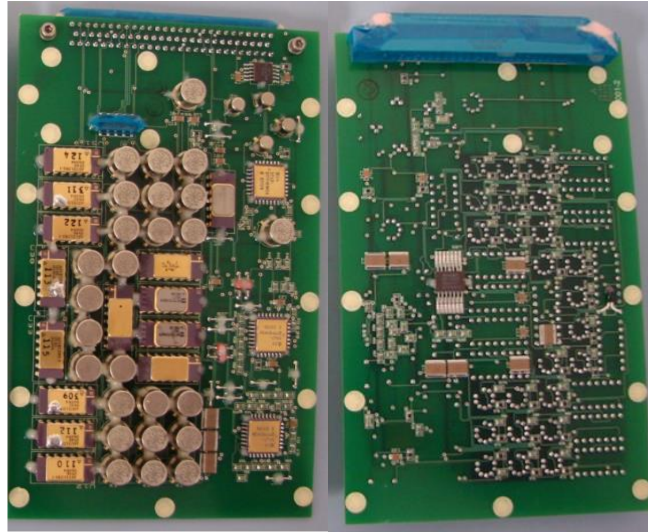

Figure 2. ELDRS instrument, front and back PCB

The die were designed and fabricated in National Semiconductor Corporation’s COTS linear bipolar process. (National Semiconductor Corporation is now Texas Instruments.) Two of the transistors on each die are gated lateral PNP (GLPNP) BJTs. Gated LPNP transistors are useful for measuring the effect of gate voltage on radiation response as well as directly measuring surface recombination. Figure 8 shows the layout of the GLPNP BJT, containing the four independent terminals: emitter, base, collector, and gate.

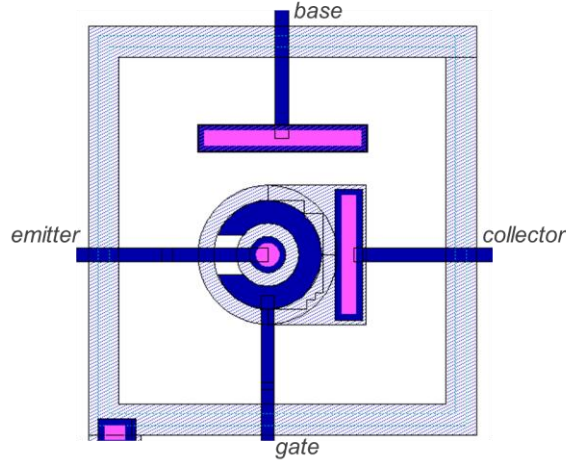

Figure 3. GLPNP layout

In addition to the two GLPNPs, each die includes a standard LPNP BJT, without gate metallization. I_B and I_C measurements for each of the 24 DUTs are obtained in sequence by sweeping the emitter voltage (base and collector grounded) from 0 V to 0.9 V in two concurrent up-down ramp cycles. Schematics of chip pad allocations for the DUTs are shown in Figure 9.

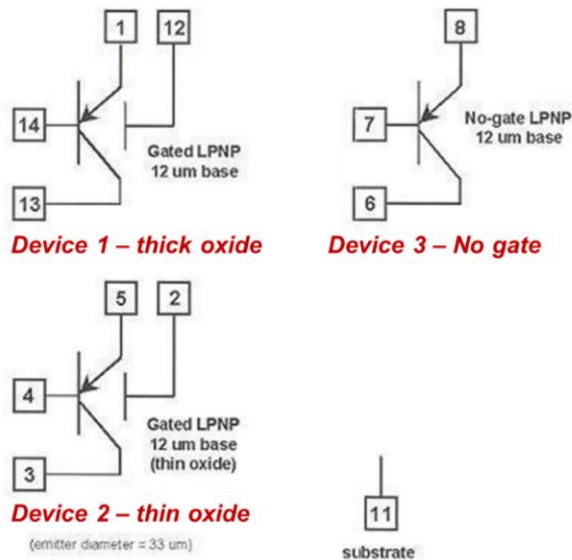

Figure 4. DUT chip pad allocations/IC pinout

V_G and oxide thickness as well as other experimental parameters have allowed for evaluation of post-rad response for different conditions. Six of the chips have a p-glass passivation layer, while the other two have a SiC passivation layer. A breakdown of the DUT types is listed in table 1. The DUTs are numbered in order of measurement. Data from DUT 1 was discarded due to excessive noise and erratic measurements that suggested an error in the chip.

Table 1. Device configurations

DUT	***Passivation***	***Package modification***
1	p-glass	unmodified
2	p-glass	modified
3	SiC	modified
4	p-glass	unmodified
5	p-glass	modified
6	p-glass	unmodified
7	SiC	modified
8	p-glass	unmodified

I_B and I_C measurements are taken as a function of base-emitter voltages (V_{EB}). For the GLPNP BJTs, four different gate voltages are applied during the V_{EB} sweeps (V_G = 6 V, 0 V, -6 V, and -12 V). The results of only two applied gate voltages, 0 V and -12 V, are discussed in this thesis.

The testboard contains the following functions: a linearly increasing voltage supply; the ability to test one BJT at a time; I-V sweeps for four gate voltages; digital logic to start,

proceed, and stop the testing once an experiment run is initiated; and latchup protection of the experiment. Once per second during testing, the carrier samples the two analog signals from the instrument. Downlinked data is transferred to Arizona State University for analysis. The DUTs are measured through a rad-hard mechanical relay multiplexer, which enables accurate low noise measurements under extreme radiation and temperature conditions. For a single DUT, there is a complex PCB operation, shown in Figure 10.

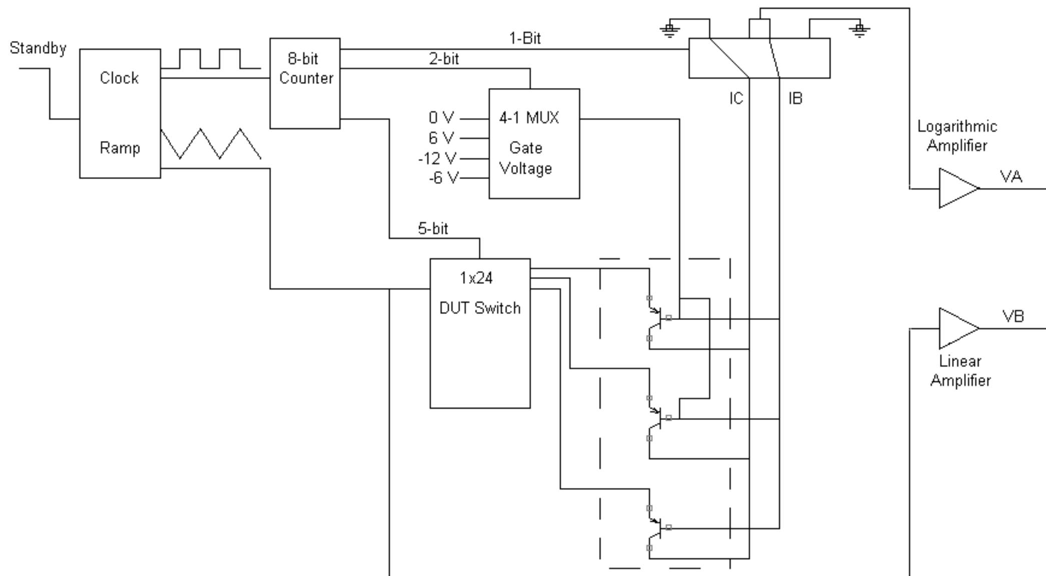

Figure 5. PCB operation for DUT measurement

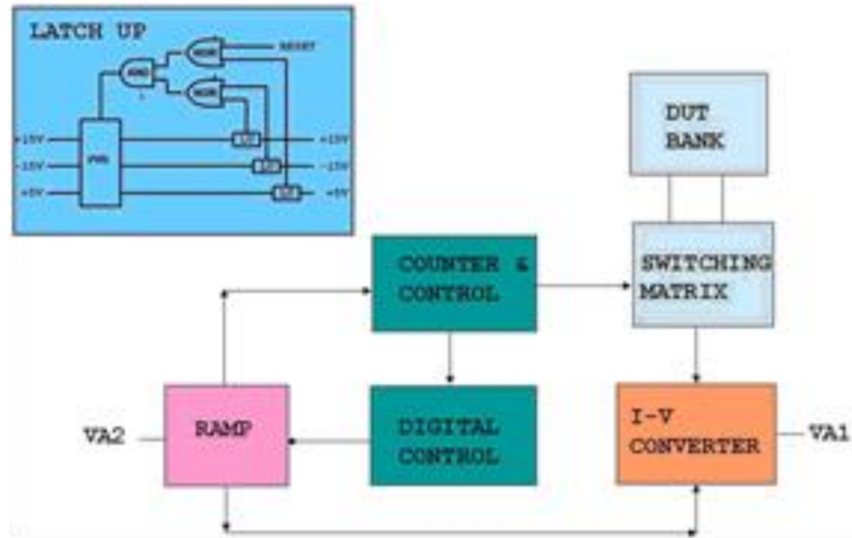

Figure 6. ELDRS flight board block diagram

The test board block diagram for the ELDRS instrument is shown in Figure 11. The latchup protection output and the reset signal control both monitor the power supply to the experiment. The DUT bank refers to the eight chips that are tested. VA2 (shown in Figure 12), a linearly increasing voltage generated by a closed loop Schmitt trigger-integrator configuration and supplied by the voltage ramp, is the V_{EB} signal to the DUTs. The counter supplies the required digital signals and is triggered through a relay by the comparator. The digital control stops the ramp when all the I-V sweeps have been performed.

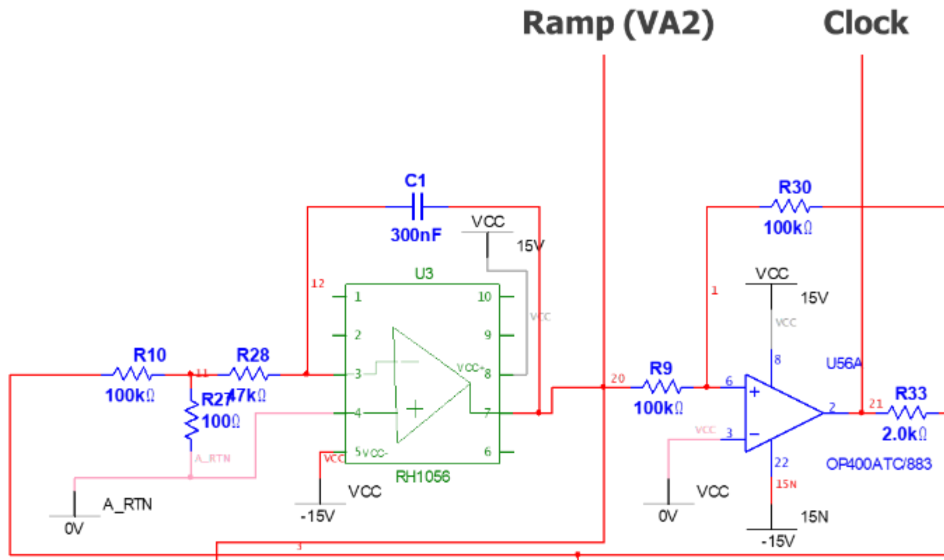

Figure 7. VA2/VRAMP schematic

The current to voltage converter (I-V converter), shown in Figure 13, allows for the current in a DUT to be sampled and recorded in the voltage domain (VA1). The I-V responses enable the characterization of low dose rate effects in the space environment. The converter is a logarithmic amplifier (logamp) that converts a logarithmic current input to a linear voltage output. The switching matrix allows for a single DUT to be selected and tested during the experiment. VA1 and VA2 are the two analog outputs that are measured in the voltage domain and recorded (the selected current of the bipolar junction transistor and the ramp voltage, respectively).

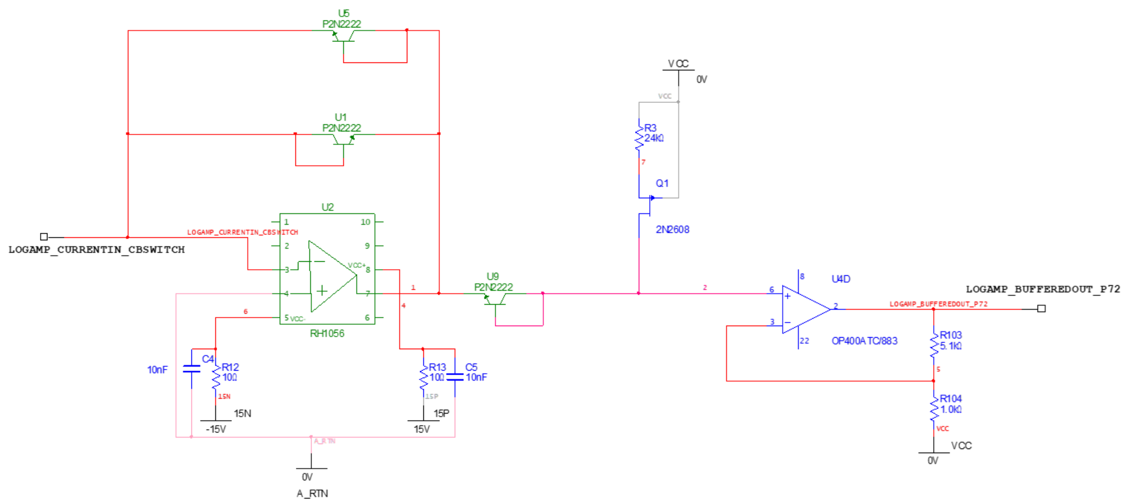

Figure 8. I-V converter schematic

When the test board is powered up with +/- 15 V and 5 V digital (provided by a separate voltage source), the counter outputs are initialized to 0 and the standby is changed from a high to low state to start the voltage ramp. These bits control the switching matrix, which selects the desired DUT. The gate voltage for the tested DUT is initially set to 0 V. After one minute, the ramp begins to produce a linearly increasing voltage to commence the testing of the first DUT. The ramp is one of the primary components of this design. It also serves as the on-chip clock.

The increment of the counter switches the DUT measurement from base current to collector current. Again, when the ramp reaches 1.0 V and resets, the counter increments and this time changes the gate voltage to 6 V. With this gate voltage, the I-V sweep is performed for the same DUT. After 2 more gate voltage changes (-6 V and -12 V) and their respective base and collector current measurements, the counter switches to the next DUT, completing the ability to test a single DUT at a time. Gate biasing during radiation exposure and measurement is performed such that the surface of the devices under the gates is held in

accumulation, depletion/weak inversion, or strong inversion. The irradiated surface state of the device is directly related to the effect ionization has on the device. Correctly biasing devices has been shown to reduce or enhance the effect of ionization damage, depending on the bias condition. Determination of biasing parameters to reduce/enhance ionization damage and the mechanisms for surface damage of the devices was investigated through this method.

After the counter reaches a total of 192 measurements (ramps), all the I-V sweeps have been completed. This triggers the encoder output to rise, which resets the counter. The board is powered off after a brief delay. The current measurements obtained during the power-off period are used for calibration purposes. The change in the encoder output results in powering off the ramp. For each full experiment run (taking approximately one minute each), other metrics such as dose and temperature are recorded. All three transistors on each IC are sampled. The ELDRS testbed output in time vs. voltage is shown in Figure 14. This graph shows the V_A from the log ramp in blue, V_B from the amp ramp in yellow, and the square clock wave in light blue. V_A is the amplified logarithmic output, base or collector current, measured at the PCB connector, while V_B is the amplified ramp output, voltage, also measured from the PCB connector.

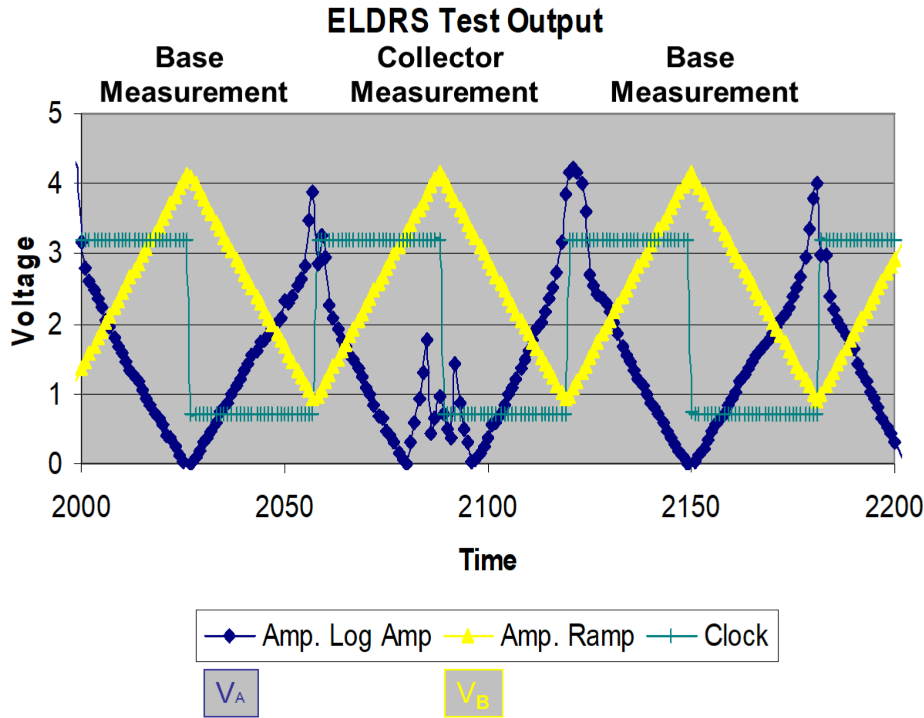

Figure 9. ELDRS test output, voltage (V) vs. time (s)

The Space Environment Testbed was flown in a complicated polar orbit (exact height unknown) composed of a mixed environment with solar particles, trapped protons, and trapped electrons all contributing to the overall dose. The experiment acquired data on the LPNP BJTs in flight continuously for twenty-two months at an average dose rate of 0.13 mrad(Si)/s, accruing a total of 7.16 krad(SiO_2). The average dose rate was reached by taking the final recorded dose and dividing it by the total time the board was in flight. Due to the occasional downtime in the board's recording and downlinking (so marked as "quiet zone" in the graph of dose vs. date, shown above), it is not possible to know the exact dose rate at every point in the experiment. The acquired dose (krad(Si)) over the analysis period is shown in Fig. Although the instrument was exposed to radiation during the "quiet zone,"

the dose during that period was not recorded. Additionally, the dose was certainly not acquired at a constant rate, due to the naturally varying makeup of the orbit in space.

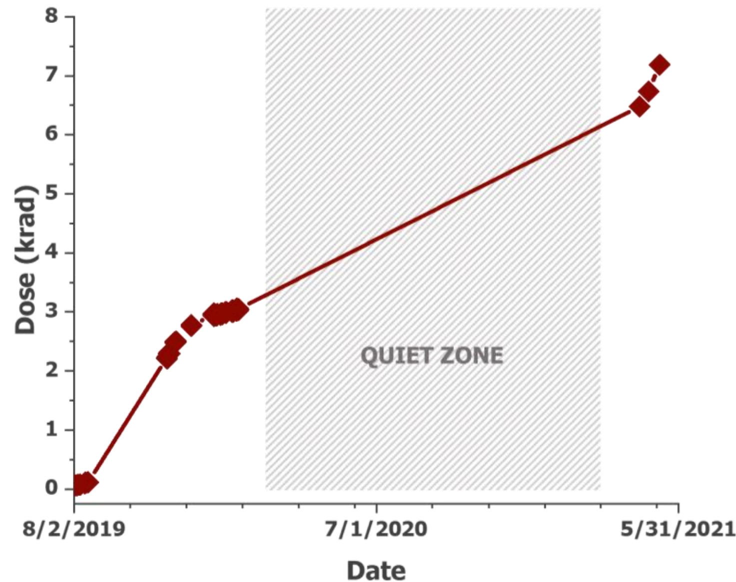

Figure 10. Accumulated average ionizing dose (krad) vs. date over the duration of the experiment

b. Data Collection and Analysis Process

This experiment measures the cumulative radiation damage (total ionizing dose and displacement damage) caused by exposure to a continuous flux of trapped particles in earth’s charged particle belts as well as the other sources mentioned above. Data from the space flight were downloaded from the testbed’s internal storage during periods of communication and manipulated to go from raw form to useable information. The analysis process involved removing noise, selecting conditions for appropriate comparison, and

plotting the log(I_B, I_C)-V_{EB} curves, a.k.a. Gummel curves. A program written in the "R" language was developed for this project to parse the raw data, label the DUT and measurement variables, and produce customizable plots and data summaries based on experiment variables such as date, temperature, and radiation dose. A sample of the graphs produced when the .zip files are uploaded to the GUI and parsed through the code is shown in Figure 16.

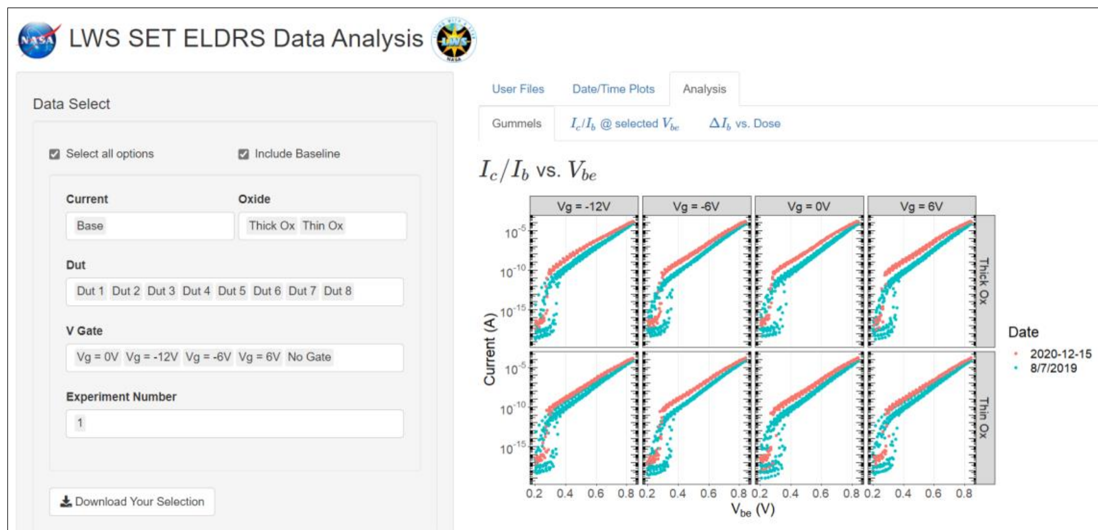

Figure 11. Data analysis GUI output

The raw data is in a form that is difficult to read; the "R" code allows the data to be downloaded in an Excel sheet with each measured variable in its own column, making it much easier to interpret the data in the form of I-V plots. The program was necessary for being able to look at the data in plain format and plot it, and also proved useful for creating a linear regression code, also written in "R," by producing data in a .csv format that was able to be input to the linear regression code. The raw-data-parsing program worked by

reading out the raw data in a sequence, associating each input with a certain variable, and finally outputting the data both in a GUI (as seen in Figure 16) which can plot the Gummel curves with various selection options and a downloadable Excel sheet with a column for each variable, neatly organized. There was some variability with the code and data which caused some difficulty. For example, if any variables were mislabeled or not taken for a certain measurement, it could knock the whole sequence out and cause variables to be mislabeled in the final product. As such, analyzing this data required careful human consideration as well as the computer program framework, ensuring that the results passed sanity checks. As always, tools can be either invaluable or useless depending on the proper knowledge of execution and usage.

One of the variables recorded for each measurement is the temperature, making it possible to separate temperature from radiation effects on the base current response. As noted in the space characteristic section, the temperature in orbit fluctuates wildly. The recorded temperatures experienced by the ELDRS testbed during the lifetime of the mission are shown in Figure 17. Possessing a range of nearly 30 K, the recorded temperature values extend from 280 K to 305 K. The LM111, an example of a commonly used COTS differential comparator, is qualified for a temperature limit of 218 K to 398 K [27], meaning it will continue to perform in those conditions but makes no promises about the added degradation which can severely shorten the lifetime of the device.

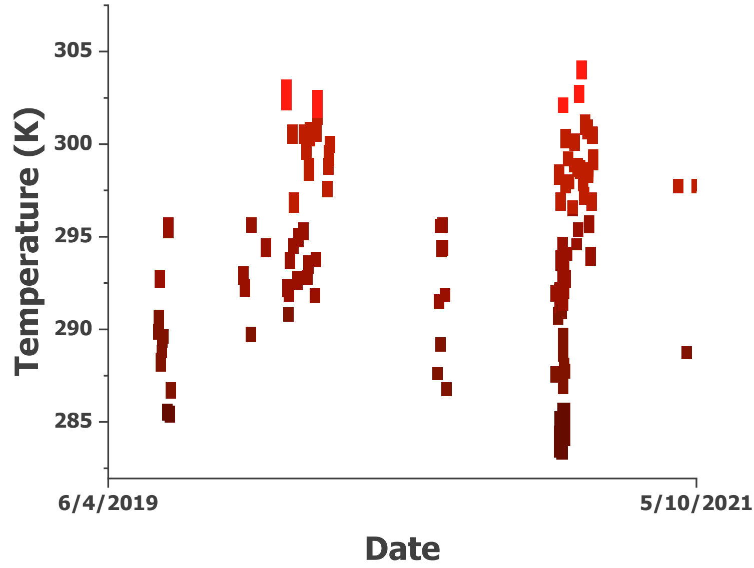

Figure 12. Temperature (K) vs. date for the duration of the experiment

Temperature has a non-negligible effect on the base current of BJT devices. To separate thermal effects from true radiation effects, a device simulation structure was created representative of the thick oxide GLPNP, shown in Figure 18.

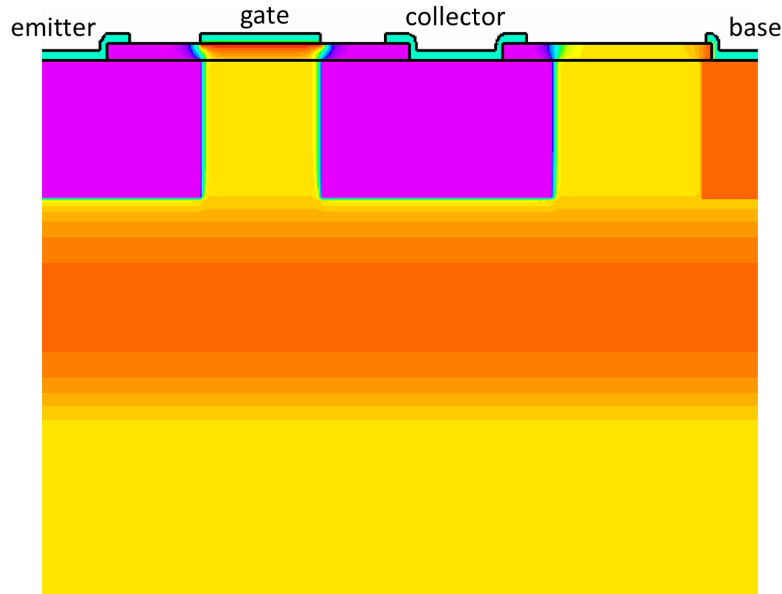

Figure 13. GLPNP thick oxide simulation structure

The structure was built and simulated using the Silvaco TCAD tool suite, with the base code written in Silvaco Deckbuild, Tonyplot for the simulations, and calculation grid (mesh) created using DevEdit. The simulated device has been shown to accurately model the base current response over a wide range of temperatures. To create the structure, the GLPNP BJT dimensions and doping profiles as well as the metal work functions were adjusted to match the actual DUT 6 device. A mesh grid was added for calculation purposes; the mesh, defining the points where calculations are performed, is more concentrated in areas of more rapid or nonuniform change in the device: around the borders of each doped region of the model as well as the metal and contacts, for fine adjustments and a higher number of calculations in those areas to result in more accurate results.

Simulation fits accurately estimate base current response at different temperatures by adjusting the *srv* parameter to post-irradiation data obtained at one temperature using the

model. Gummel characteristics obtained through the simulation were shown to accurately reproduce the pre-irradiation data over temperatures ranging between 280 K – 305 K (the range experienced by the experiment in space).

CHAPTER 4

EXPERIMENTAL RESULTS

a. ELDRS results

i. Overview of the ELDRS Phenomemon

Although the ionizing radiation mechanisms discussed above hold true for BJTs at every rate, at lower dose rates there is an increase in degradation that is not observed by high dose rate testing. This was a surprising discovery as compared to metal-oxide-semiconductor (MOS) devices, also commonly used in Earth and space circuits, where degradation is reduced at LDR, and HDR can accurately predict LDR results [21]. This LDR response in bipolar devices, called enhanced low dose rate sensitivity (ELDRS), makes testing and flying BJTs particularly difficult. This also points to the necessity of more space data for BJTs in particular, since MOS devices do not exhibit this phenomenon. ELDRS, at this point in time a well-known effect in BJTs, is characterized by the relative increase in degradation in transistors and circuits when exposed to radiation at decreased dose rates as compared to relative high dose rates. Degradation during low dose rate (LDR) irradiation is considerably greater than what is observed after post-rad anneal, signifying a true dose rate effect [28].

ELDRS is a space charge effect. At high dose rates free and trapped holes build up in the oxide, suppressing the transport of holes and positively charged protons. However, at low dose rates the transports of these species is not suppressed. This mobility leads to much greater buildup of interface traps and trapped holes near the interface after irradiation [29]. In circuits using BJTs, such as the LM111 voltage comparator, gain degradation in the

input transistors is the primary cause of increases in I_B [22], necessitating a thorough understanding of the degradation process.

Figure 19 [5] shows the relative damage vs. dose rate for selected transistors. The sharp decline in the slope for the LM111 and LM324, both PNPs (as many common operational amplifiers and comparators), is notable for how much more damage is present at the very low doses. Additionally, this graph demonstrates how very low the dose rate must be to test for maximum damage in PNPs. Dose rate damage saturates for NPN style transistors at approximately an order of magnitude higher than that for high dose rates, and the slope only continues to increase for PNP devices as dose rates get lower, making low dose rate testing and understanding a high priority for mission survival rates. The fact that the slope shows no sign of slowing or saturation in PNP devices is of great concern in LDR testing.

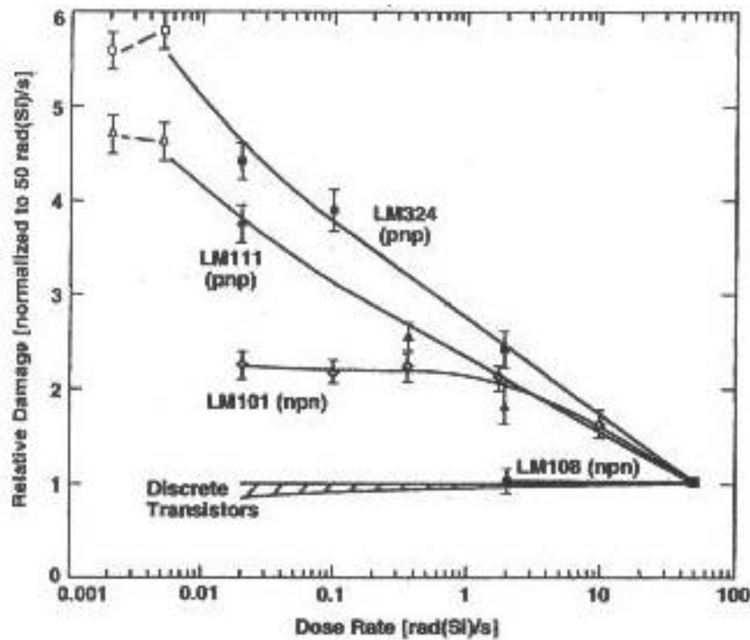

Figure 14. Relative damage vs. dose rate (rad(Si)/s)

Although manufacturing differences cannot be accounted for and do cause variations in dose rate response, PNP transistors tend to display this heightened sensitivity across several parts, and the data shown here are representative of most PNP devices. [5].

Recent research has shown that the surrounding hydrogen content in packages also affects BTJ radiation response, primarily by introducing species critical to interface trap passivation and de-passivation [30]. Un-passivated interface traps increase surface recombination in BJTs, leading to precipitous increases in base current and reduced current gain [30]. The ELDRS experiment used two different types of passivations, silicon carbide (SiC) and p-glass, in order to compare the effects of LDR irradiation on the two different passivation layers.

ii. ELDRS Experiment Results

The ELDRS testbed performed I_B measurements on each transistor (as previously described), which were used to calculate ΔI_B for DUT 6: GLPNP, p-glass passivation, unmodified package, thick oxide, with gate metallization, base current measured at $V_G = 0$ V. The data were gathered from the space run, downloaded and parsed as described previously; processed via removing noise selecting the correct temperature and package conditions; and compared to ground-based test results previously published in literature [40, 21, 31, 30] DUT 6 was chosen as it had a large amount of available data in the chosen temperature range of 298-302 K, the data was comparably less noisy, and the data passed sanity checks; i.e., pre-rad measurements do not change, I_C does not change from pre-rad

to post-rad (as it should not be affected by irradiation, unlike I_B), and I_B does change post-rad.

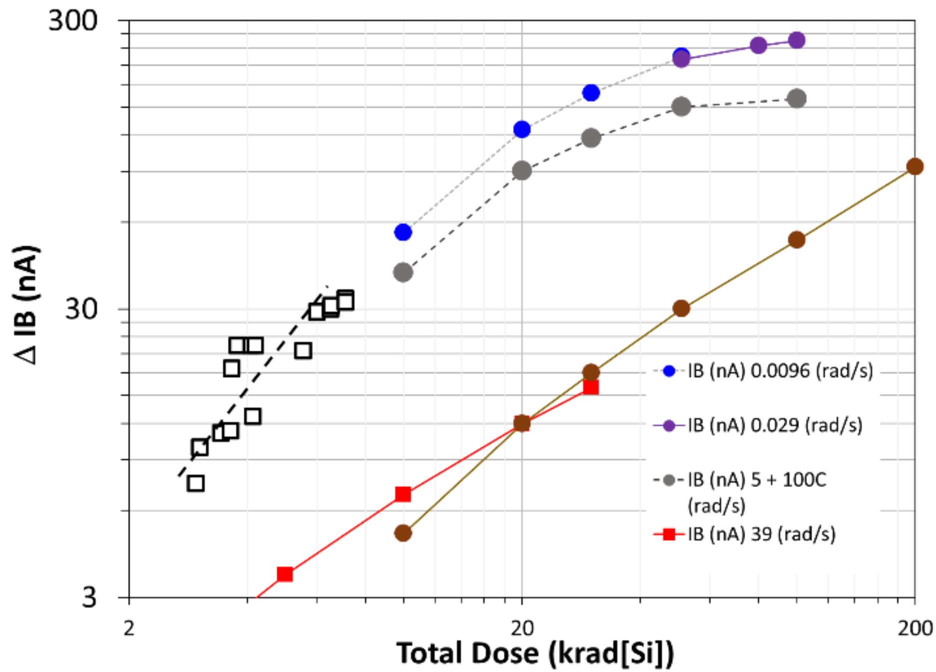

Figure 15. ΔI_B (nA) vs. total dose (krad(Si)) for the duration of the experiment

Fig 21 shows the DUT 6 on-orbit data for ΔI_B on the same plot as ground-based low dose rate (<30 mrad/s), elevated temperature irradiation (5 rad/s + 100° C), and high dose rate (≥39 rad/s) ground test data. Although I_B was used to compare the package variants, ΔI_B (procured by subtracting a chosen baseline value from I_B) was chosen for this comparison as the published ground-based data used ΔI_B. The black dashed line with square, white-filled markers shows the DUT 6 transistor space data for ΔI_B vs. dose. These data were measured at an on-board temperature ambient of ~300 K, chosen for being approximately the same temperature as the ground-based tests. These space data were actually taken at

various temperatures, but have been adjusted using the previously mentioned GLPNP model to simulate results for 300 K. The on-orbit ΔI_B is increasing as dose increases, following an upward slope that trends toward that of the ground-based LDR data. The ΔI_B increase in the space data (measured at an V_{EB} = 0.5 V, the same emitter-base voltage as the ground-based tests) is likely due to the buildup of radiation-induced traps at the BJT base oxide-silicon interface [32, fleetwood 1997], as discussed earlier. The space environment data trendline for ΔI_B is already significantly higher than the HDR ground-based data at the same dose levels; indeed, the on-orbit data appear to be closely tracking the LDR ground-based data slope. These space-data results demonstrate, for the first time, the ELDRS effect on BJTs fabricated in a COTS linear bipolar circuit process.

b. Package and Test Condition Variables

In addition to the ELDRS analysis, Gummel plots (log(I_C) and I_B versus V_{EB}) from selected DUTs are compared with each other to assess the impact of different experimental parameters (listed in table 2). The graphs shown below in Figures 22-25 plot I_B vs. dose for each device to examine the post-rad effects of package and measurement variables irradiation on base current response. The gate voltage can be used to enhance or suppress ionizing radiation response [33]. For these parts, only gate voltages above 5 V seem to effectively suppress the effects of TID-induced interface traps, so for V_G = 0 V, it is assumed that the ionizing effects are dominant. Table 2 lists each experimental parameter and its variation, with each parameter detailed below the table. The multiple experimental

variables as well as the large quantity of data have been key in performing data analysis for this experiment.

Analysis of the data has determined that among all the device variables the surface potential and oxide thickness have the greatest impact on base current degradation, in accordance with previously published results [34, 1]. The base current response due to irradiation on individual BJTs manufactured in an integrated linear bipolar process has been well-documented in ground-based studies [6, 10, 21, 36, 40, 19, 34]. The mission data from this experiment have been published in [36, 37]. Externally, temperature fluctuations have the biggest impact on the base current. This is a well-documented effect in BJTs, and has also been shown in this experiment using a linear regression code, detailed in chapter 4.

Table 2. Variables associated with experimental parameters

Experimental Parameter	***Variation***
Radiation dose	Pre-rad/post-rad
Temperature	Temperature fluctuations
Gate voltage	0 V and -12 V
Package modification	Modified and unmodified
Passivation	P-glass and silicon carbide
Oxide thickness	Thick oxide and thin oxide

Prerad: A very low dose exposure shortly after the experiment launch. This is essentially “pre-irradiation,” from 0.06 to 0.11 krad, from the beginning of the experiment. These data were recorded from 8/02/2019 to 8/18/2019. This dose is too low to have any significant

impact on the base current response of the transistor, and so was chosen as a baseline for changes post-exposure.

Postrad: The highest dose acquired by the end of the experiment, reaching ~7 krad. These data were recorded for a total time of 22 months.

Temperature: As expected, the BJT base and collector currents change with temperature. The extreme temperature fluctuations posed a significant challenge for this analysis by affecting ΔI_B; to avoid seeing thermal effects, each data set is for the initial results are plotted at a specific temperature. Each temperature is within 2 K of the temperature noted in the plot title. These data were analyzed prior to the finalization of the GLPNP temperature simulation model, so these data were all taken at the actual reported temperature.

Gate Voltage: Results are reported for test voltages of V_G = 0 V and -12 V. The standby irradiation bias for all DUTs is 0 V on all terminals. 0 and -12 V were chosen to examine the impact of negative gate bias on surface recombination velocity, due to the high depletion mode achieved with -12V.

Modified Package: Some packages were modified at the time of receipt to release the hydrogen; although the exact hydrogen content is not known, the modified packages were assumed to have a slightly lower in-package hydrogen content then the unmodified package.

Unmodified Package: Assumed high in-package hydrogen content, ~1%. This has been dismissed as a variable since linear bipolar circuits are known to have a hydrogen response [30] and none was observed in this case. The parts in this experiment sat for a long time before measurement and therefore the hydrogen was assumed to have leaked out.

Passivation: P-glass or silicon carbide (SiC) passivation, deposition method unknown. Passivation is known to have an effect on radiation response [ref – see above] by affecting the buildup of traps on the oxide surface.

Thick oxide: 1.22 µm.

Thin oxide: 0.56 µm.

Each set of Gummel plots contains the prerad and postrad V_{EB} versus I_B and I_C for each parameter as noted in the Figure and caption. I_C does not change appreciably with irradiation, as expected, whereas I_B does, also as expected. This as well as the lack of change in I_B and I_C in the prerad data serve as a sanity check for the data. These data are shown in Figures 22-25. Each parameter comparison is shown at $V_G = 0$ V and $V_G = -12$ V, to easily compare the differences between gate voltages for each selected condition.

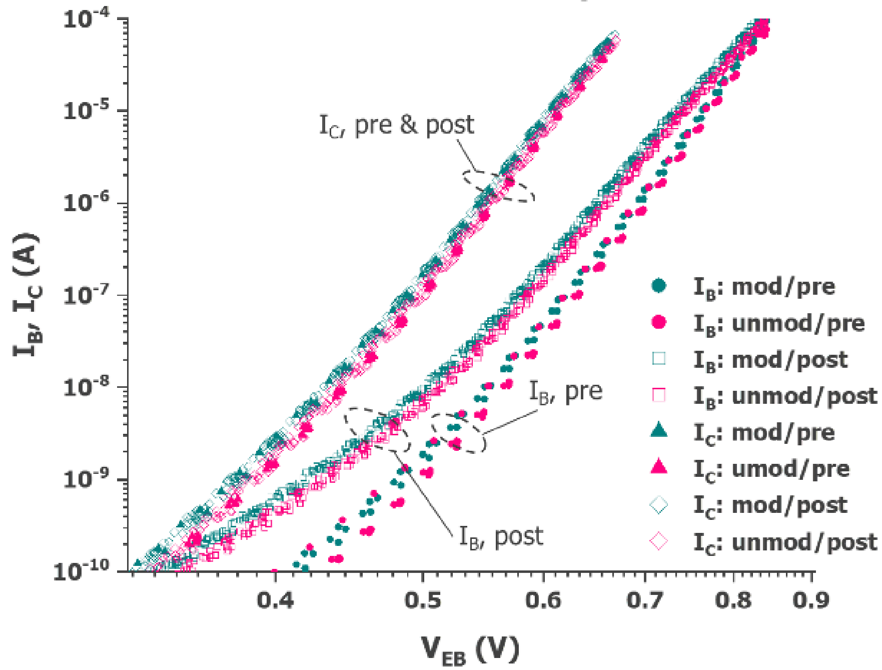

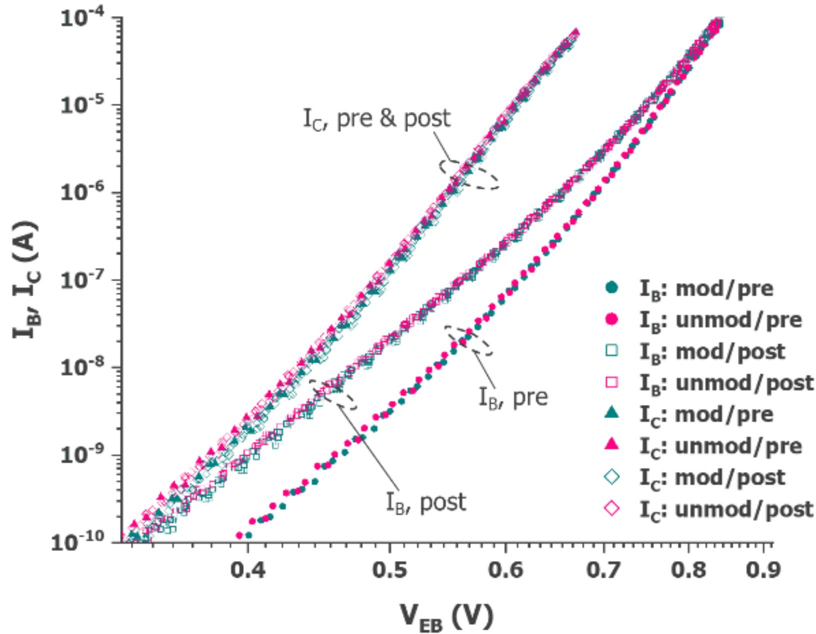

Figure 16. Thick oxide, modified p-glass vs. unmodified p-glass, 0V and -12V

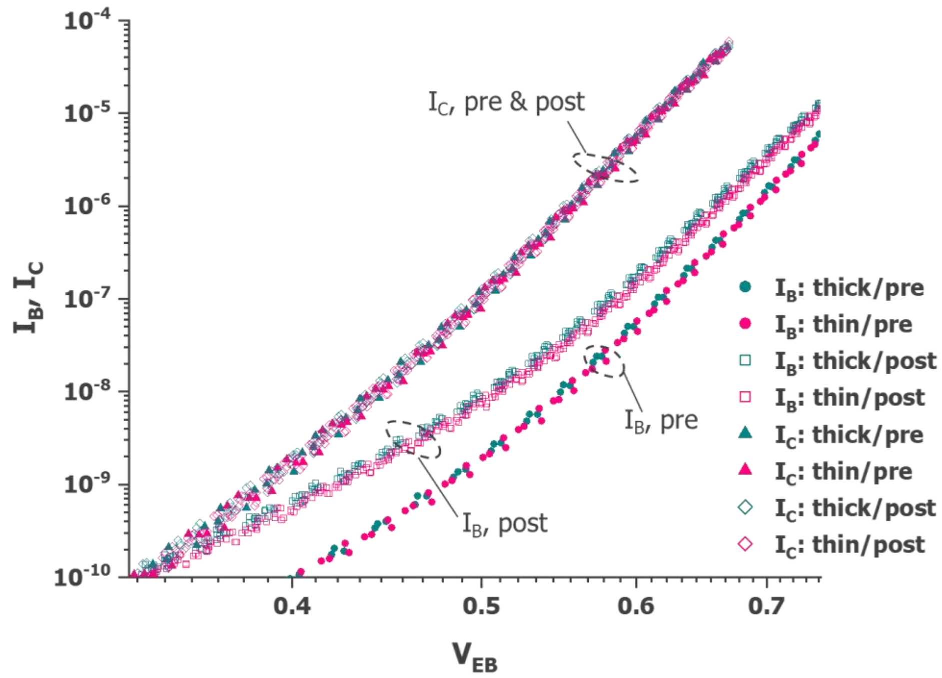

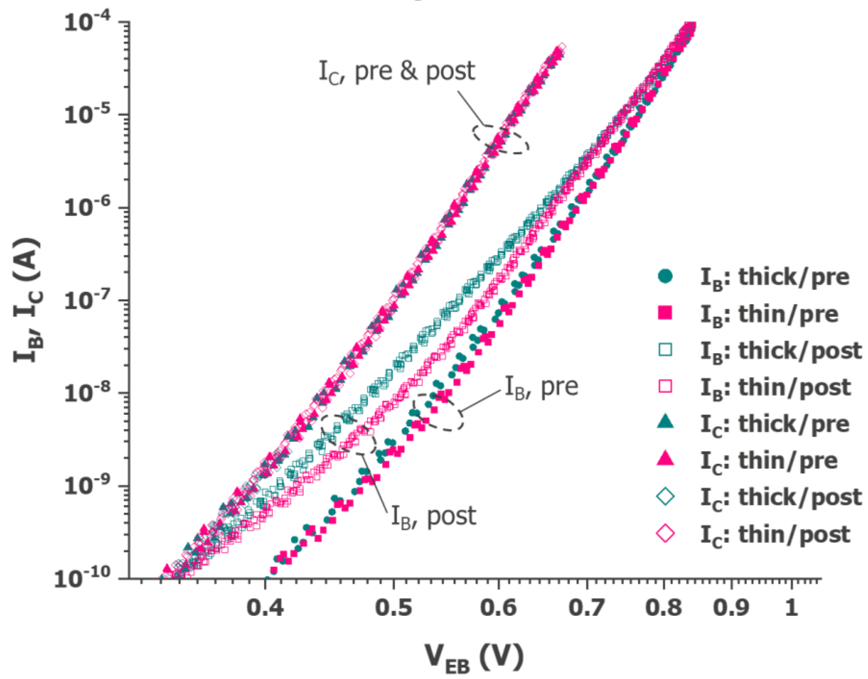

Figure 17. SiC modified package, thick oxide vs. thin oxide, 0V and -12V

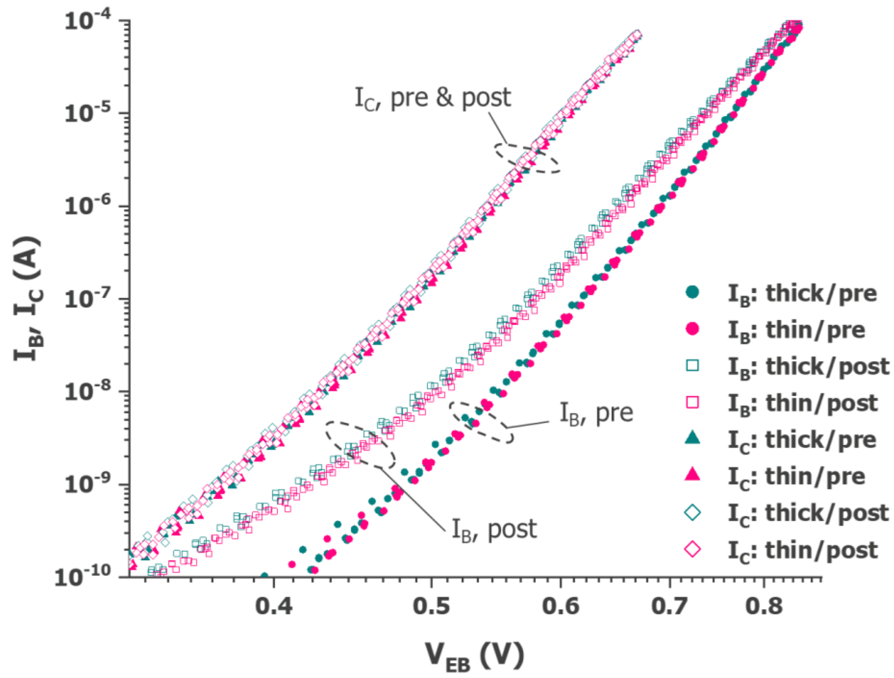

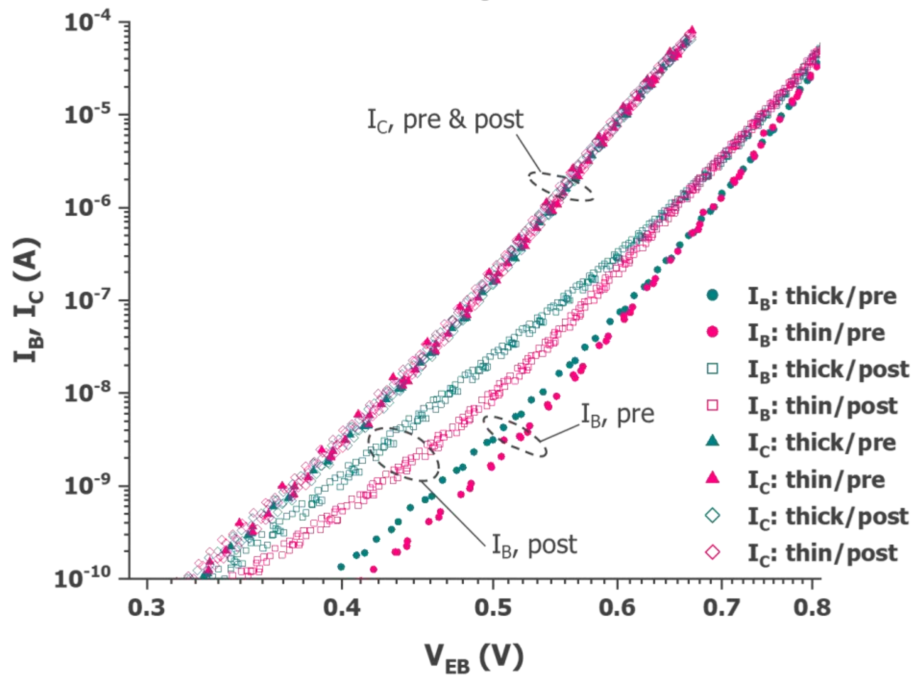

Figure 18. P-glass modified package, thick oxide vs. thin oxide, 0V and -12V

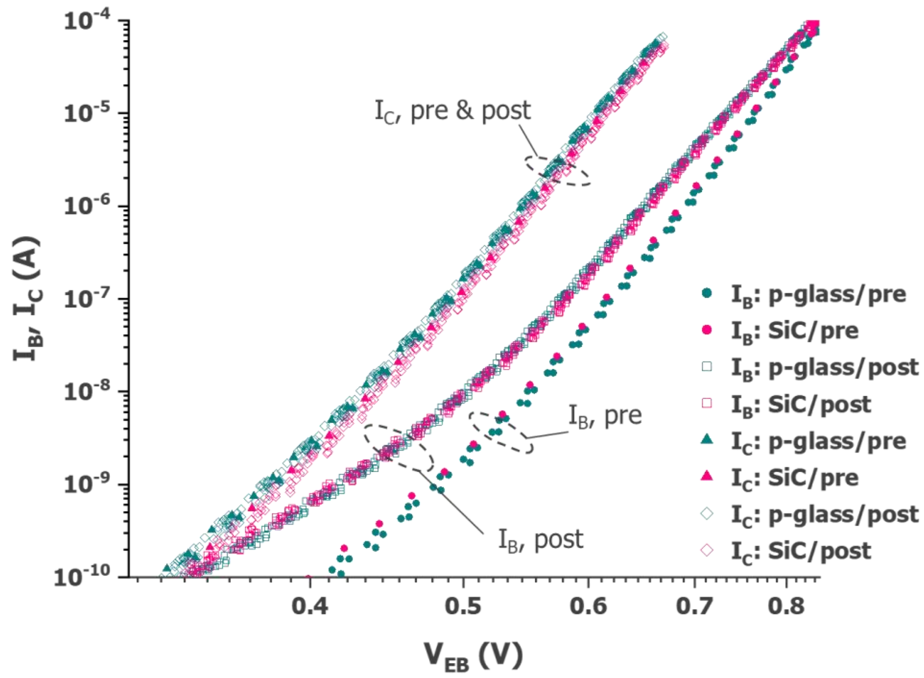

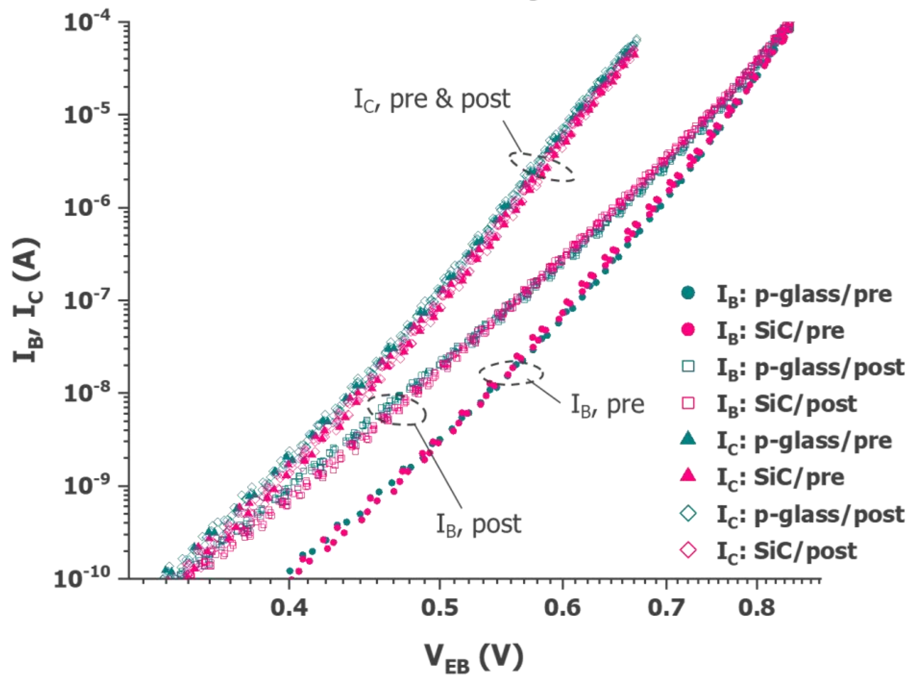

Figure 19. Thick oxide, p-glass modified vs. SiC modified, 0V and -12V

Figure 21 indicates that base current degradation is not a strong function of the package type (i.e., modified or unmodified) in this case. The (un)modified package variants were selected to monitor the possible effect of in-package hydrogen concentration, which is known to have a significant effect on BJT radiation response [28, 30, 34]. The fact that there is very little difference between modified and unmodified packages, for either bias, indicates that there is not a large difference in the hydrogen content. Although the modified package was modified with the intent of capturing the effect of the packaging hydrogen content on the radiation response (degradation), the parts ended up sitting unused for quite a while during which time the hydrogen presumably diffused from the unmodified package as well as the modified.

Figure 24 reveals that there is very little difference in the responses for the p-glass and SiC passivations, regardless of gate bias. This suggests that the passivation, at least for these two passivation types, does not have an impact on increasing base current in irradiated BJTs. It is known that passivation can affect the total dose response, likely by changing the mechanical stress response [38] and affecting the number of traps that are able to build up on the surface, but more studies are done comparing SiC and silicon (Si), since SiC has properties that not only reduce TID response as compared to Si but also has a higher lattice energy and thus also reduces displacement damage, resulting in reduced overall degradation [39]. [38] also discusses a p-glass/nitride combination vs. no passivation as well as other passivations, showing that common passivation layers reduce TID sensitivity. From this evidence, a tentative conclusion can be drawn that the appropriate material should be chosen for other desirable properties depending on the application and not for TID damage reduction in this case of p-glass vs. SiC.

The comparisons of thick oxide versus thin oxide have notable results. The difference for post-rad vs. pre-rad for both the p-glass and SiC (Figures 23 and 24) show no difference between the I_B curves at $V_G = 0$ V, but do show a noticeable difference at $V_G = -12$ V. The increase in base current depends directly on the interface traps (N_{IT}) and oxide trapped charge (N_{OT}) (N_{OT} not discussed herein). Analyzing the interface traps with relation to the increase in base current could reveal much about the distribution of traps that build up with exposure, as discussed in the next section.

c. SRV and NIT Extraction

Among the most destructive defects caused by ionizing radiation are interface traps (N_{IT}), which increase surface recombination and lead to a precipitous rise in base current [6, 10, 11]. A measured change in I_B can provide insight to the buildup of these traps via extraction of the BJT's surface recombination velocity (*srv*), which shifts with the buildup of traps; *srv* can then be plugged into an analytical model to obtain a quantitative measurement of the N_{IT} buildup [25]. Recombination is the dominant post-irradiation mechanism of base current in a BJT [24, 6, 10].

In order to calculate the N_{IT} from base current and evaluate the change in surface recombination velocity, we must first extract *srv* at a given dose level. Analytically, *srv* can be related to TID-induced based current:

$$srv \cong \frac{2I_B}{qn_iP_Ex_{dB}\exp\left(\frac{V_{EB}}{2V_T}\right)} \quad (2).$$

While this analytical model, as well as others, have been shown to reproduce the effects of radiation on base current [11, 25], it was determined that computer simulation was much better at accurately capturing the complex physics of thermal effects on these parts. Thus, the TCAD simulation on the GLPNP structure was used for extracting *srv* rather than relying on the analytical model. *SRV* is inversely proportional to the interface trap density, as shown by equation 1 above.

Figure 25 shows the fits to the based data at multiple mission dose levels (0.06, 2.21, and 5.65 krad(Si)), all simulated to an adjusted junction temperature of 300 K using the TCAD GLPNP model.

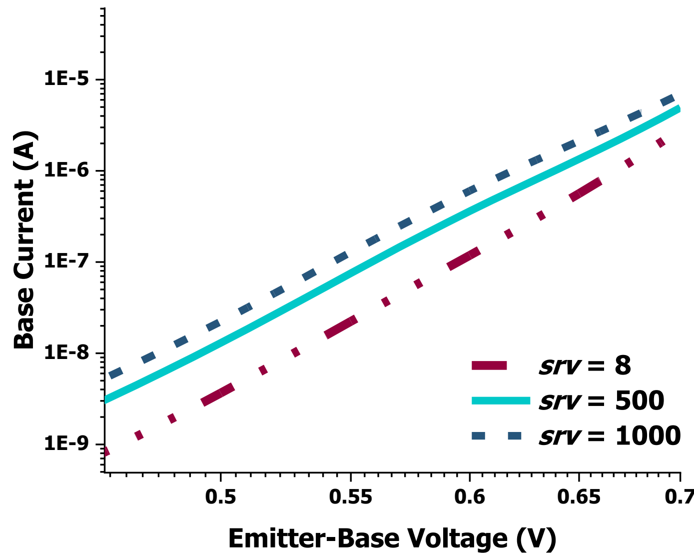

Figure 20. Simulated I_B vs. V_{EB} for T=300 K

The *srv* values obtained at the four selected doses are listed in table 3. Although another *srv* could have been included with the additional dose accumulated after this analysis was

performed, it was found that there was little difference in the final results from 5.65 krad to 7 krad.

Table 3. Dose and corresponding *srv* values

Dose (krad(Si))	***Surface Recombination Velocity (cm/s)***
0.06	100
2.21	500
3.68	800
5.65	1000

After extracting *srv* and characterizing the changes over dose, these data can be used to extract N_{IT} buildup as a function of TID using the relationship

$$N_{IT} \cong (\sigma v_{th})^{-1} * srv \quad (3),$$

where σ = 2.3x10-16 [11]. Figure 26 plots the extracted N_{IT} vs. dose.

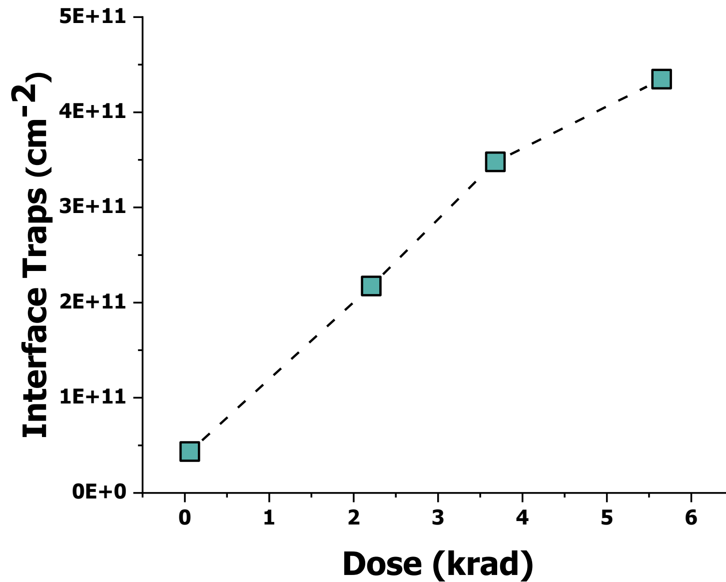

Figure 21. N_{IT} (cm^{-2}) vs. dose (krad)

This plot clearly shows a positive slope, indicating an increase in NI_T as dose increases. It is known that interface traps build up at the oxide interface junction, increasing recombination rate by providing additional sites where recombination can occur. The increased degradation occurring when the higher dose correlates with V_G = -12 V provides some insight into the exact location of the buildup of these traps. The oxide thickness specifically under the emitter metal wing, shown in Figure 27 and highlighted by the red circle, is likely the same for the thin and thick oxide variants. However, the metal emitter in the center, designated by the large yellow arrow, is significantly thicker in the thick oxide package.

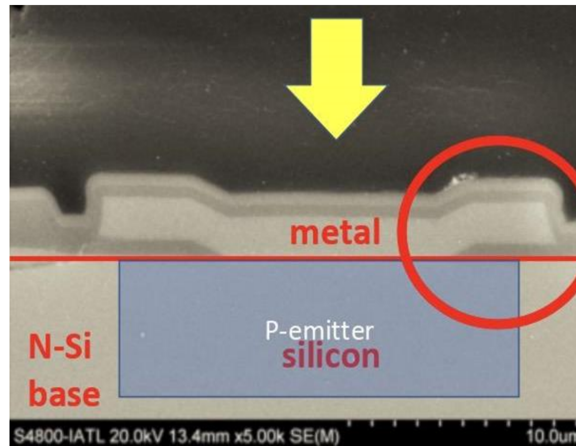

Figure 22. NPN metal-oxide connection

When $V_G = 0$ V is applied, interface traps under the wing region likely dominate the response since much of the emitter-base depletion region is located there, as excess base current is typically caused by recombination current in the depletion region.

However, when $V_G = -12$ V is applied to the gate, the depletion region will expand from under the wing and spread toward the thicker oxide in the center due to the high negative voltage. The part itself is forward biased with $V_{EB} > 0V$ during the V_{EB} sweep from 0V to 1V. A qualitative, not-to-scale diagram is shown in Figures 29 and 30, where the depletion region is represented by the dashed line in the p- and n-doped regions.

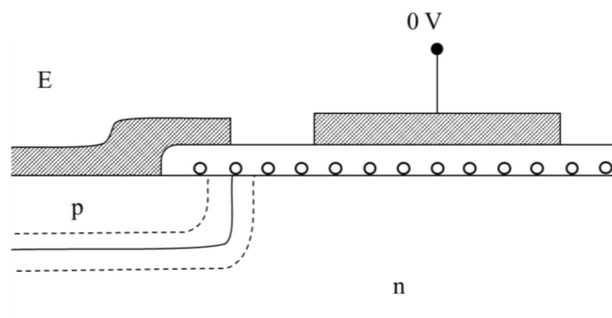

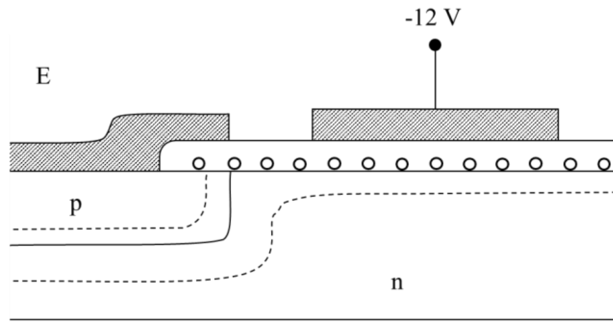

Figure 23. Thin oxide at V_G = 0 V and -12 V

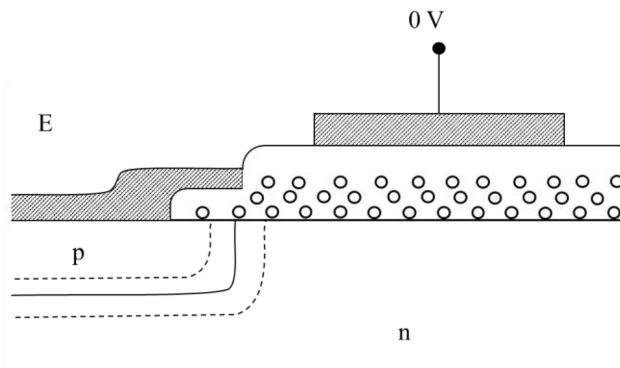

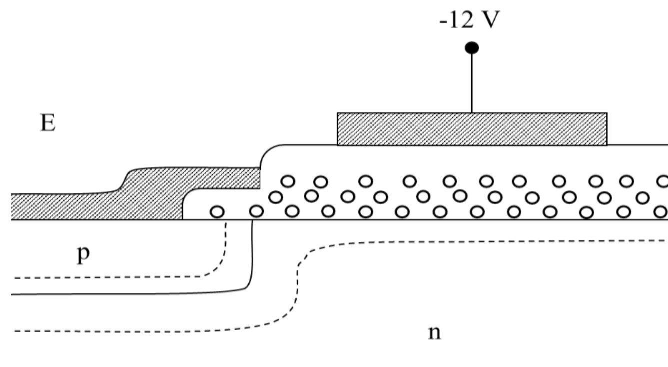

Figure 24. Thick oxide at V_G = 0 V and -12 V

The expansion in the depletion region makes the interface traps in the thick or thin bipolar base oxide in the varying center region effective contributors to the excess base current, instead of only including the traps under the wing. The amount of interface traps under the thick oxide should be greater [35, 40]. The depletion region spreads into the n-type base, relatively lightly doped compared to p-type regions. The traps are negatively charged, causing the depletion region to spread into the n-type base region [6].

This is a potential explanation for the difference in thin versus thick oxide *srv*/recombination rate only when V_G = -12 V is applied. The total charge in the accumulation layer is proportional to the oxide charge, and the depth of accumulation layer is dictated by the amount of radiation-induced charge buildup [10]. The expanded depletion region allows the higher buildup of charge in the thick oxide to interact with more of the free charge in the depletion region, increasing net recombination rate at the surface. For the -12 V case, the depletion region is extending all the way across, allowing the interface traps to make contact with the depletion region across the entire device. This effect occurs in both thin and thick oxides; however, the thick oxide is able to contain more charge, as seen in Figure 29. This extra charge is likely what causes the recombination rate to increase.

d. Linear Regression Analysis

The combined effect of the degradation mechanisms (both via temperature and radiation) and packaging differences on current gain in BJTs is nonlinear. Not only are the degradation mechanisms from both TID and DD difficult to quantify individually due to the complex interaction of net positive oxide trapped charge and *srv* [6], but the combined

effect of excess positive oxide trapped charge (N_{OT}) and the interface traps discussed above (N_{IT}) are nonlinear [22]. One way to separate these effects is through modeling. Another way to possibly separate these effects, or at least gain awareness as to which variables are correlated, is through a linear regression analysis. Linear regression reveals collinearity, which can provide clues as to which mechanism is causing the primary degradation in certain situations. Linear regression is a type of modelling approach that does not require a TCAD device model, but rather groups the data in a relationship between a known independent variable and one or more dependent variables. Linear regression analysis can also show the variance of a certain variable from the predicted line, revealing the effect of a single variable on a predicted (ideal) curve.

For this thesis, a linear regression code was written in "R" to analyze the variance among the variables and see which variables were most correlated both with each other and with degradation of base current via the Gummel plots. The data was binned by passivation, temperature, pre- and post-rad, and V_G. Shown below in Figures 31 and 32 are graphs from a linear regression analysis performed with various independent and dependent variables to examine the effect of the different variables on the radiation response by binning the package variations. Figure 30 shows the Gummel plot for all GLPNP DUTs, pre-rad and post-rad (as designated by dark blue and light blue respectively) for temperatures at 300 K +/- 2 K and both passivations, oxide thicknesses, and V_G values. This plot shows the distinct increase in base current post-irradiation, regardless of temperature, oxide thickness, passivation, or applied gate voltage.

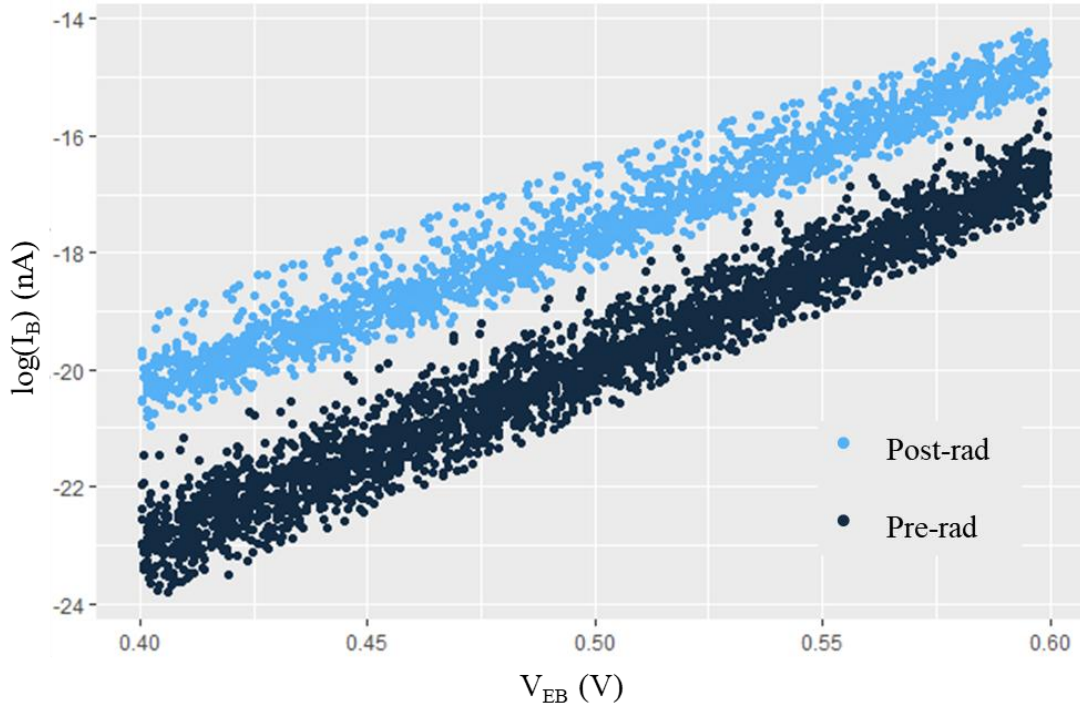

Figure 25. Log(I_B) (nA) vs. V_{EB} (V), GLPNP, pre- and post-irradiation

Figure 31 shows the Gummel plot for post-irradiation, temperatures at 300 K +/- 2 K, grouped by thick oxide/thin oxide and $V_G = 0$ V/$V_G = -12$ V. This plot shows the noticeable grouping of I_B for the $V_G = -12$ V case and thick oxide condition, demonstrating the significant difference for the -12 V/thick oxide combination. This corroborates the increase in degradation at -12 V and reinforces the conclusion that the depletion region is spreading to include more of those interface traps where recombination rate probability is much higher and causing increase in base current.

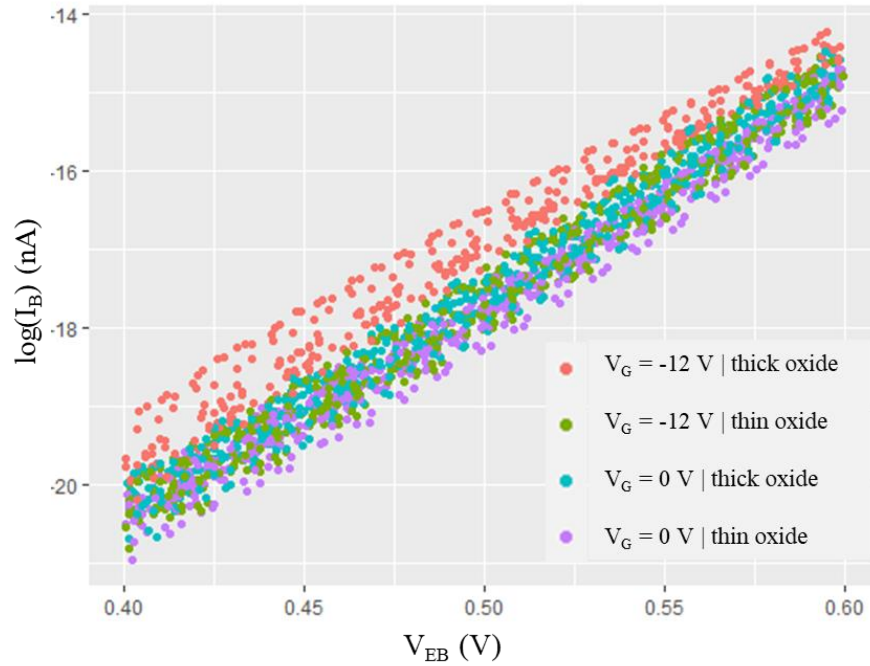

Figure 26. Log(I_B) (nA) vs. V_{EB} (V), GLPNP, post-irradiation

The linear regression data, while providing similar results to the manual plots and comparisons done above in the parametric comparisons, provide more insight to the trends in this data by way of being able to compile all the data in a way that a single person could not accessibly perform. Further analysis of this method and resulting data is ongoing.

CHAPTER 5

CONCLUSION

Space environment effects on BJTs are becoming increasingly important as the quest to expand humankind past Earth demands a a full understanding of these effects. While gated BJTs are mostly an experimental device and not always applicable to the specific devices used in spacecraft, the analysis of the ionizing radiation-induced degradation on the GLPNP BJTs leads to a better understanding of the degradation in commerically used BJTs. The temperature and ionizing radiation experienced by these parts in the space environment both cause degradation in BJTs that can lead to shortened part lifetime or total part failure. This thesis examines both the environmental hazards and the degradation effects of those hazards on the gated BJTs flown in a harsh space orbit.

Examining ELDRS specifically is paramount to understanding degradation in lateral bipolar devices, as they are particularly susceptible to low dose rate effects. Comparing the ideal performance of BJTs, ground-based high dose rate data, and space-based low dose rate data furthers understanding of the mechanisms behind ELDRS, validates current ground-based testing methods, and will lead to improved environmental models in the future. Comparing the parametric variables also provides insight to how different packages can affect the radiation response. The combination of the V_{EB}= -12V and thick oxide part shows the increased surface recombinaton velocity which leads to the increase in base current. The N_{IT} extraction using the *srv* calculations and the TCAD GLPNP model also validate generally accepted theories of the depletion region expansion across the device. While these results are already strong, the future addition of the linear regression analysis will be able to perform these variable comparisons for the entire set of

data for each variable, including secondary or tertiary variables that will continue to illuminate the specific devices behind LDR degradation in LPNP BJTs. These results were published in the IEEE NSREC 2021 Data Workshop, SmallSat Conference Proceedings 2021, HEART Conference Proceedings 2022, and IEEE Aerospace Conference Proceedings 2022.

REFERENCES

[1] R. N. Nowlin, E. W. Enlow, R. D. Schrimpf, and W. E. Combs, "Trends in the Total-Dose Response of Modern Bipolar Transistors," IEEE Trans. Nucl. Sci, vol. 39, pp. 2026-2035, 1992.

[2] S. McClure, R. L. Pease, W. Will, and G. Perry, "Dependence of Total Dose Response of Bipolar Linear Microcircuits on Applied Dose Rate," IEEE Trans. Nucl. Sci., vol. 41, pp. 2544-2549, 1994

[3] R. L. Pease, W. E. Combs, A. Johnston, T. Carriere, and S. McClure, "A Compendium of Recent Total Dose Data on Bipolar Linear Microcircuits," 1996 IEEE Radiation Effects Data Workshop Record, vol. No. 96TH8199, pp. 28-37, 1996.

[4] J. L. Barth, C. S. Dyer, and E. G. Stassinopoulos, "Space, Atmospheric, and Terrestrial Radiation Environments," IEEE Trans. Nucl. Sci., vol. 50, pp. 466-482, 2003.

[5] A. H. Johnston, B. G. Rax, and C. I. Lee, “Enhanced damage in linear bipolar integrated circuits at low dose rate,” *IEEE Trans. Nucl. Sci.*, vol. 42, pp. 1650-1659, 1995.

[6] S. L. Kosier, R. D. Schrimpf, R. N. Nowlin, D. M. Fleetwood, M. DeLaus, R. L. Pease, W. E. Combs, A. Wei, and F. Chai, "Charge Separation for Bipolar Transistors," IEEE Trans. Nucl. Sci., vol. 40, pp. 1276-1285, 1993.

[7] Staff Writers. “NASA Aims to Put Man on Mars by 2037.” 24/7 Space News. SPACEDAILY, September 24, 2007. Accessed November 30, 2022. https://www.spacedaily.com/reports/NASA_aims_to_put_man_on_Mars_by_2037_999.html.

[8] J. L. Titus, D. Emily, J. F. Krieg, T. Turflinger, R. L. Pease, and A. Campbell, “Enhanced low dose rate sensitivity (ELDRS) of linear circuits in a space environment,” IEEE Trans. Nucl. Sci., vol. 46, pp. 1608-1615, 1999.

[9] T. L. Turflinger, A. B. Campbell, W. M. Schmeichel, J. F. Kreig, J. L. Titus, M. Reeves, P. W. Marshall, and R. L. Pease, “ELDRS in Space: An Updated and Expanded Analysis of the Bipolar ELDRS Experiment on MPTB,” IEEE Trans. Nucl. Sci., vol. accepted for publication, 2003.

[10] D. M. Schmidt, A. Wu, R. D. Schrimpf, D. M. Fleetwood, and R. L. Pease, "Modeling Ionizing Radiation Induced Gain Degradation of the Lateral PNP Bipolar Junction Transistor," IEEE Trans. Nucl. Sci., vol. 43, pp. 3032- 3039, 1996.

[11] H. J. Barnaby, C. Cirba, R. D. Schrimpf, S. L. Kosier, P. Fouillat, and X. Montagner, "Modeling BJT Radiation Response with Non-uniform Distributions of Interface Traps," IEEE Trans. Nucl. Sci., vol. 47, pp. 514-518, 1999.

[12] “Catalog of Earth Satellite Orbits.” NASA. NASA, September 4, 2009. Accessed November 30, 2022. https://earthobservatory.nasa.gov/features/OrbitsCatalog/page2.php.
[13] Multiple Authors. “Background: Trapped Particle Radiation Models.” SPENVIS. Accessed November 30, 2022. https://www.spenvis.oma.be/help/background/traprad/traprad.html.
[14] Dr. Tony Phillips. “Van Allen Probes Discover a New Radiation Belt.” NASA, Februrary 28, 2013. Accessed November 30, 2022. https://science.nasa.gov/science-news/science-at-nasa/2013/28feb_thirdbelt/

[15] S. Bourdarie and M. Xapsos, “The Near-Earth Space Radiation Environment,” IEEE Trans. Nucl. Sci., vol. 55, 2008.

[16] B.R. Bhat, N. Upadhyaya, and R. Kulkarni, “Total Radiation Dose at Geostationary Orbit,” IEEE Trans. Nucl. Sci., vol. 52, 2005.

[17] J.H. Adams, Jr., A.J. Tylka, and B. Stiller, “LET Spectra in Low Earth Orbit,” IEEE Trans. Nucl. Sci., vol. NS-33, 1986.

[18] OMERE 5.6.1.3, TRAD, August 10, 2003.

[19] M.R. Shaneyfelt, J.R. Schwank, et al., “Annealing Behavior of Linear Bipolar Devices With Enhanced Low Dose Rate Sensitivity,” IEEE Trans. Nucl. Sci., vol. 51, 2004.

[20] R.L. Pease, L.M. Cohn, et al., “A Proposed Hardness Assurance Test Methodology for Bipolar Linear Circuits and Devices in a Space Ionizing Radiation Environment,” IEEE Trans. Nucl. Sci., vol. 44, 1997.

[21] D.M. Fleetwood, S.L. Kosier, et al., “Physical Mechanisms Contributing to Enhanced Bipolar Gain Degradation at Low Dose Rates,” IEEE Trans. Nucl. Sci., vol. 41, 1994.

[22] H.J. Barnaby, C. Cirba, et al., “Modeling BJT Radiation Response with Non-Uniform Energy Distributions of Interface Traps,” IEEE Trans. Nucl. Sci., vol. 47, 2000.

[23] R.F. Pierret, “Semiconductor Device Fundamentals,” Addison Wesley, 1996.

[24] B.G. Streetman, “Solid State Electronic Devices,” 2nd Edition, Prentice-Hall, 1979.

[25] H.J Barnaby, B. Vermiere, and M.J. Campola, “Improved Model for Increased Surface Recombination Current in Irradiated Bipolar Junction Transistors,” IEEE Trans. Nucl. Sci., vol. 62, 2015.

[26] A.H. Johnston, G.M. Swift, and B.G. Rax, “Total Dose Effects in Conventional Bipolar Transistors and Linear Integrated Circuits,” IEEE Trans. Nucl. Sci., vol. 41, 1994.

[27] Texas Instruments, “LM111, LM211, LM311 Differential Comparators Datasheet,” Rev. K, March 2017.

[28] R.L. Pease, P.C. Adell, et al., “The Effects of Hydrogen on the Enhanced Low Dose Rate Sensitivity (ELDRS) of Bipolar Linear Circuits, IEEE Trans. Nucl. Sci., vol. 55, 2008.

[29] H.J. Barnaby, Arizona State University, Tempe, AZ, private communication, Fall 2022.

[30] P.C. Adell, B. Rax, I.S Esqueda, and H.J. Barnaby, “Hydrogen Limits for Total Dose and Dose Rate Response in Linear Bipolar Circuits,” IEEE Trans. Nucl. Sci., vol. 62, 2015.

[31] R.N. Nowlin, R.L. Pease, et al., “Evaluating TM1019.6 ELDRS Screening Methods Using Gated Lateral PNP Transistors,” IEEE Trans. Nucl. Sci., vol. 52, 2005.

[32] X.J. Chen, H.J. Barnaby, et al., “Nature of Interface Defect Buildup in Gated Bipolar Devices Under Low Dose Rate Irradiation,” IEEE Trans. Nucl. Sci., vol. 53, 2006.

[33] D.R. Ball, R.D. Schrimpf, and H.J Barnaby, “Separation of Ionization and Displacement Damage Using Gate-Controlled Lateral PNP Bipolar Transistors,” IEEE Trans. Nucl. Sci., vol. 49, 2002.

[34] X.J. Chen, H.J. Barnaby, et al., “Mechanisms of Enhanced Radiation-Induced Degradation Due to Excess Molecular Hydrogen in Bipolar Oxides,” IEEE Trans. Nucl. Sci., vol. 54, 2007.

[35] P. Cazenave, P. Fouillat, X. Montagner, H. Barnaby, R. D. Schrimpf, L. Bonora, et al., "Total Dose Effects on Gate Controlled Lateral PNP Bipolar Junction Transistors," IEEE Transactions on Nuclear Science, vol. 45, pp. 2577-2583, 1998.

[36] H.J. Barnaby, A. Benedetto, C. Cook, and M.J. Campola, “First Results from BJT Enhanced Low Dose Rate Sensitivity (ELDRS) Experiment on NASA Space Environment Testbed,” MRQW 2020.

[37] A.R. Benedetto, H.J. Barnaby, et al., “BJTs in Space: ELDRS Experiment on NASA Space Environment Testbed,” IEEE Radiation Effects Data Workshop, 2021.

[38] M.R. Shaneyfelt, R.L. Pease, et al., “Passivation Layers for Reduced Total Dose Effects and ELDRS in Linear Bipolar Devices,” IEEE Trans. Nucl. Sci., vol. 50, 2003.

[39] P. Hazdra, S. Popelka, “Displacement damage and total ionisation dose effects on 4H-SiC power devices,” Selected Papers from the 14th International Seminar on Power Semiconductors, The Institution of Engineering and Technology, 2018.

[40] R.L. Pease, D.G. Platteter, et al., "Characterization of Enhanced Low Dose Rate Sensitivity (ELDRS) Effects Using Gated Lateral PNP Transistor Structures, IEEE Trans. Nucl. Sci., vol. 51, 2004.